JOURNAL OF GEOPHYSICAL RESEARCH, VOL. 103, NO. B1, PAGES 783–810, JANUARY 10, 1998

New and refined constraints on three-dimensional Earth structure from normal modes below 3 mHz

Joseph S. Resovsky and Michael H. Ritzwoller

Department of Physics and Cooperative Institute for Research in the Environmental Sciences
University of Colorado, Boulder

Abstract. We present the results of generalized spectral fitting (GSF) regressions which estimate normal mode structure coefficients for the observable spheroidal and toroidal free oscillation multiplets below 3 mHz. The size, accuracy, and precision of our new catalogue of modal constraints make it a powerful new tool for assessing and refining three-dimensional Earth models. The estimates include more than 3100 coefficients for 90 multiplets and 25 pairs of coupled multiplets, including several deep mantle overtones previously obscured by fundamental modes. The coefficients constrain mantle structures of both even and odd spherical harmonic degrees, through degree 12 in some cases. Improvements in accuracy and precision have been achieved with three innovations: the development of GSF, an enhancement of the established spectral fitting technique which incorporates both Coriolis and structural coupling between multiplets; the application of GSF to an edited, high signal-to-noise and geographically diverse data set of more than 4500 seismograms from 33 high moment earthquakes; and the assignment of coefficient uncertainties using a Monte Carlo method to simulate the effects of seismic noise, theoretical errors, and coefficient covariances. The results of GSF are assessed by examining the internal consistency of estimated coefficients and through comparisons with recent mantle models. The new catalogue of structure coefficients and uncertainties is available as an electronic supplement to this paper and through the University of Colorado internet site.

1. Introduction

1.1. Research Program

The past decade has seen a dramatic increase in the quantity and distribution of broadband seismographic stations and the occurrence of several very strong earthquakes (Figure 1), which have yielded thousands of new high signal-to-noise ratio seismograms. These data provide the opportunity for much more detailed analyses of the Earth's free oscillation spectrum than have been attempted to date. Comparisons of recent three-dimensional global seismic models reveal significant discrepancies which emphasize the need for additional normal mode constraints on aspherical structure. Such constraints can be used to assess existing models and address persistent questions about correlations and scalings between variations in v_s, v_p, ρ, and topography on internal boundaries [e.g., *Ritzwoller and Lavely,* 1995]. For these reasons, we have made our goal the establishment of a new, higher-quality, and greatly expanded catalogue of normal mode structure coefficients, which serve to constrain three-dimensional Earth structure.

This paper presents the first major steps in this program: (1) the development of generalized spectral fitting (GSF), an enhancement of the established spectral fitting technique [*Ritzwoller et al.,* 1986, 1988; *Giardini et al.,* 1987, 1988; *Li et al.,* 1991; *Widmer et al.,* 1992a,b; *Tromp and Zanzerkia,* 1995; *He and Tromp,* 1996], which incorporates intermultiplet coupling through aspherical structure and the Coriolis force, (2) the assembly of an expanded data set of $\sim$ 4500 edited broadband seismograms from 33 strong earthquakes (Table 1), (3) the application of GSF to these data to obtain estimates of more than 3100 normal mode structure coefficients from 90 different multiplets with frequencies below 3 mHz (Figure 2 and Table 2), and (4) the development of a Monte Carlo method of error analysis and other tools for assessing and quantifying the accuracy and precision of the coefficient estimates. Most of the multiplets analyzed sample heretofore poorly constrained structures in the transition zone and lower mantle. Thus the new coefficient estimates provide an important complement to existing body and surface wave data. They also establish the utility of GSF, which may be employed in future analyses of the normal mode spectrum above 3 mHz.

Paper number 97JB02482.
0148-0227/98/97JB-02482$09.00

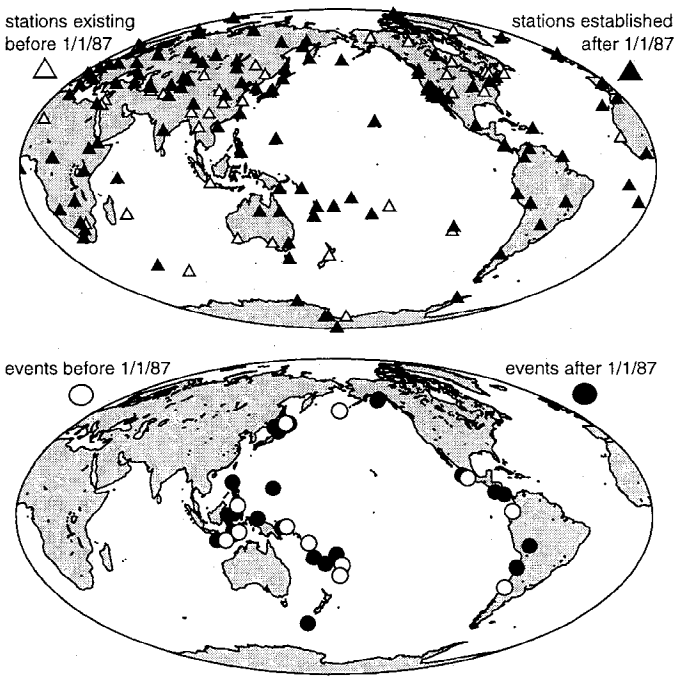

Figure 1. Geographical distribution of the sources and receivers employed. There has been a marked increase in the number of events and stations employed compared to those used, for example, by *Ritzwoller et al.* [1988].

1.2. Motivation

Individual free oscillations, or normal mode singlets, are clustered into usually unresolved spectral multiplets composed of modes with similar wavelengths and nearly degenerate frequencies. These multiplet peaks characterize typical normal mode spectra, such as that shown in Figure 3a. Broadband digital seismic data became readily available in the late 1970s and early 1980s. To take advantage of these data, the techniques of singlet stripping [*Ritzwoller et al.*, 1986; *Widmer et al.*, 1992a] and spectral fitting [*Giardini et al.*, 1987, 1988; *Ritzwoller et al.*, 1986, 1988; *Li et al.*, 1991] were developed. These methods were used to observe the splitting of singlet frequencies that was expected to be the dominant effect of aspherical Earth structure on isolated fundamental and overtone multiplets. The observations were reported as structure (or interaction) coefficients, which are nonlinearly related to the observed multiplet spectra but are linear functionals of Earth structure. These new constraints on three-dimensional (3-D) Earth structure were employed in the construction of only a few mantle models, including SH.10c.17 [*Masters et al.*, 1992] and S16B30 [*Masters et al.*, 1996]. The utility of structure coefficients estimated with spectral fitting was limited by the relatively small number of multiplets analyzed, by the isolated multiplet approximation, which ignored some important information in normal mode amplitude spectra and confined the modal constraints to even-degree structures, and by inaccuracies resulting from structures unspecified in the regressions, which estimated only the few longest wavelengths of aspherical structure.

Most recent 3-D Earth models, including S12_WM13 [*Su and Dziewonski*, 1994], MK12_WM13 [*Dziewonski and Su*, 1995], and SAW12D [*Li and Romanowicz*, 1996], have been constrained to fit only body and surface wave data. Models that incorporate normal mode constraints, such as S16B30, have used structure coefficients that are, for the most part, almost a decade old. Synthetic seismograms generated from such models fit long-period seismic spectra much more poorly than do synthetics constructed using our normal mode structure coefficient estimates, as demonstrated by Figures 3b and 3c. Comparisons of models, like those of Figure 4, indicate poor correlations in the transition zone and lower mantle, which are not as well sampled by body and surface waves as are other regions other regions of the mantle. In contrast, most of the normal

Table 1. Earthquakes

Index	Date	Location	Moment, 10^{20}Nm
1	June 22, 1977	Tonga	21.3[a]
2	Aug. 19, 1977	South of Sumbawa	40.5[a]
3	Dec. 6, 1978	Kuril Islands	6.4
4	Dec. 12, 1979	Ecuador Coast	19.6[a]
5	July 17, 1980	Santa Cruz Islands	4.8
6	June 22, 1982	Banda Sea	1.7
7	March 28, 1983	New Ireland	4.6
8	Nov. 20, 1984	Mindanao	2.2
9	March 3, 1985	Central Chile	10.1[a]
10	Sept. 19, 1985	Michoacan	10.6[a]
11	May 5, 1986	Andreanof Islands	12.0[a]
12	Oct. 20, 1986	Kermadec Islands	4.5
13	Nov. 30, 1987	Gulf of Alaska	10.0[a]
14	March 6, 1988	Gulf of Alaska	5.2[a]
15	May 23, 1989	Macquarie Islands	21.6[a]
16	March 3, 1990	South of Fiji	3.0
17	April 18, 1990	Minahassa	3.3
18	July 16, 1990	Luzon	4.1
19	Dec. 30, 1990	New Britian	1.8
20	April 22, 1991	Costa Rica	3.3
21	Sept. 2, 1992	Nicaragua	3.4
22	Oct. 11, 1992	Vanuatu	1.5
23	Dec. 12, 1992	Flores Islands	5.5[a]
24	Jan. 15, 1993	Hokkaido	2.7
25	July 12, 1993	Hokkaido	5.7[a]
26	Aug. 8, 1993	South of Mariana	5.5[a]
27	March 9, 1994	Fiji Islands	3.1[a]
28	June 2, 1994	South of Java	5.3
29	June 9, 1994	North Bolivia	27.8[a]
30	Oct. 4, 1994	Kuril Islands	28.7[a]
31	Dec. 28, 1994	East of Honshu	4.0
32	July 30, 1995	Northern Chile	16.4[a]
33	Oct. 9, 1995	Jalisco	11.5

[a]GSF moment estimate. Other moments are from the Harvard CMT catalogue.

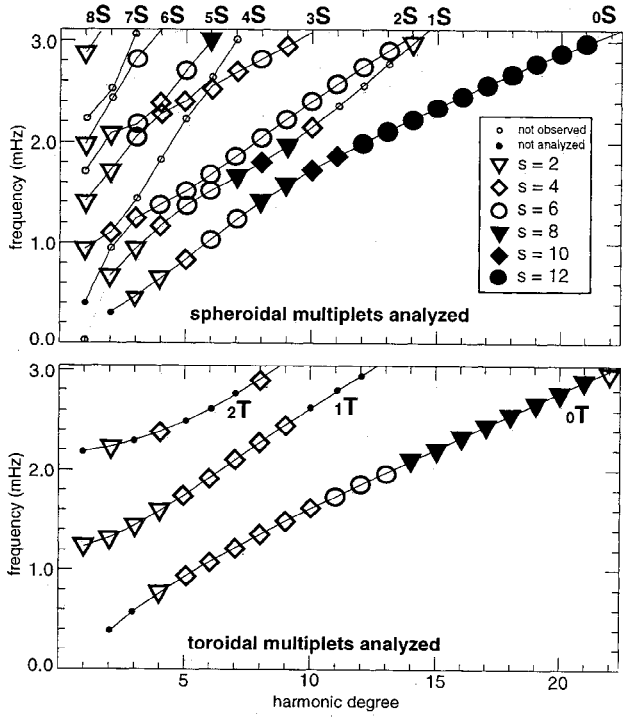

Figure 2. Dispersion diagrams displaying the multiplets analyzed in this study. The type of symbol indicates the maximum degree of structure coefficient reported for each multiplet.

modes below 3 mHz exhibit strong sensitivity to structures at these depths, as demonstrated by the sensitivity kernels included on Plate 1. For this reason, detailed normal mode constraints from this spectral regime can serve as useful tools for (1) assessing existing models of both 1-D and 3-D v_s and v_p structures in the mantle [e.g., *Ritzwoller and Lavely,* 1995], (2) performing new inversions for 3-D models, which may be constrained to be geodynamically consistent [e.g., *Forte et al.,* 1994; *Ritzwoller and Wahr,* 1994], and (3) exploring the possibility of obtaining independent models of aspherical density structures [e.g., *Ritzwoller and Wahr,* 1995]. Such constraints are provided by the catalogue of normal mode structure coefficients presented here.

Section 2 explains the relation between self- and cross-coupling structure coefficients and Earth structure and describes GSF regressions. Section 3 discusses the means by which we have enhanced the accuracy and precision of the normal mode catalogue. The results of the GSF analyses are presented in section 4. Section 5 describes the Monte Carlo simulations we use to assign uncertainties. Section 6 discusses the potential application of the new catalogue to the development of future generations of 3-D Earth models.

2. Methodology

2.1. Normal Mode Coupling

A spherically symmetric, nonrotating, anelastic, and isotropic (SNRAI) Earth model may be represented by the expression $\mathbf{m}_0(r) = [\kappa_0(r), \mu_0(r), \rho_0(r)]$, where κ and μ are the complex bulk and shear moduli. In this case, an aspherical Earth model is described by $\mathbf{m}(\mathbf{r}) = \mathbf{m}_0(r) + \delta\mathbf{m}(r,\theta,\phi)$, and by a set of two-dimensional perturbations, $h_d(\theta,\phi)$, to the radii of discontinuities (r_d) in the structural parameters. These perturbations to the spherical model may be represented as sums of spherical harmonic components:

$$\delta\mathbf{m}(\mathbf{r}) = \sum_{s,t} [\delta\kappa_s^t(r), \delta\mu_s^t(r), \delta\rho_s^t(r)] Y_s^t(\theta,\phi) \,, \qquad (1)$$

and

$$h_d(\theta,\phi) = \sum_{s,t} h_{sd}^t Y_s^t(\theta,\phi) \,, \qquad (2)$$

where s (≥ 0) and t ($|t| \leq s$) index the harmonic degree and azimuthal order, respectively, of the complex spherical harmonics, $Y_s^t(\theta,\phi)$, which are normalized according to the convention of *Edmonds* [1960].

Free oscillation multiplets of the SNRAI model are identified by the type (spheroidal, S, or toroidal, T), radial order (n), and harmonic degree (l), of their eigenfunctions. Each multiplet $k \equiv (\text{type}, n, l)$ comprises $2l+1$ degenerate singlet modes, referred to by azimuthal index m. Assuming that aspherical perturbations to Earth structure are relatively small, the singlets of a ro-

Table 2. GSF Frequency and Q estimates

Modes	Frequency, (μHz)	$f - f^{\text{PREM}}$, (μHz)	Q	$Q - Q^{\text{PREM}}$
${}_0S_3$	468.594 ± 0.10[a]	0.03	383 ± 25[b]	-34
${}_0S_4$	646.882 ± 0.10	-0.20	373 ± 17	0
${}_0S_5$	840.009 ± 0.10	-0.43	358 ± 12	2
${}_0S_6$	1037.540 ± 0.05	-0.69	342 ± 6	-4
${}_0S_7$	1231.040 ± 0.05	-0.77	351 ± 10	9
${}_0S_8$	1412.850 ± 0.05	-0.68	347 ± 5	9
${}_0S_9$	1577.550 ± 0.10	-0.75	342 ± 8	9
${}_0S_{10}$	1725.650 ± 0.11	-0.84	343 ± 5	15
${}_0S_{11}$	1861.280 ± 0.13	-1.15	340 ± 8	18
${}_0S_{12}$	1989.180 ± 0.10	-1.21	339 ± 5	24
${}_0S_{13}$	2111.630 ± 0.11	-1.32	322 ± 5	15
${}_0S_{14}$	2230.070 ± 0.10	-1.34	317 ± 5	19
${}_0S_{15}$	2345.040 ± 0.13	-1.36	314 ± 5	25
${}_0S_{16}$	2457.020 ± 0.14	-1.21	308 ± 6	29
${}_0S_{17}$	2566.200 ± 0.13	-0.93	305 ± 7	36
${}_0S_{18}$	2672.460 ± 0.12	-0.85	296 ± 5	37
${}_0S_{19}$	2776.150 ± 0.20	-0.84	283 ± 5	34
${}_0S_{20}$	2877.780 ± 0.10	-0.60	280 ± 5	39
${}_0S_{21}$	2977.260 ± 0.10	-0.48	270 ± 5	38
${}_0T_4$	765.996 ± 0.15	0.32	268 ± 22	40
${}_0T_5$	928.366 ± 0.10	0.11	254 ± 16	37
${}_0T_6$	1079.084 ± 0.10	0.24	249 ± 34	43
${}_0T_7$	1221.003 ± 0.10	0.29	207 ± 11	12
${}_0T_8$	1356.553 ± 0.17	0.43	201 ± 10	14
${}_0T_9$	1487.070 ± 0.17	0.45	191 ± 15	11
${}_0T_{10}$	1613.666 ± 0.41	0.39	175 ± 19	2
${}_0T_{11}$	1737.418 ± 0.20	0.56	171 ± 10	4
${}_0T_{12}$	1858.819 ± 0.17	0.87	168 ± 10	5
${}_0T_{13}$	1977.878 ± 0.18	0.88	162 ± 10	3
${}_0T_{14}$	2095.429 ± 0.18	1.06	158 ± 10	3
${}_0T_{15}$	2211.157 ± 0.40	0.80	155 ± 10	3

Table 2. (continued)

Modes	Frequency, (μHz)	$f-f^{\text{PREM}}$, (μHz)	Q	$Q-Q^{\text{PREM}}$
${}_0T_{16}$	2326.403 ± 0.27	1.20	148 ± 10	0
${}_0T_{17}$	2440.317 ± 0.31	1.21	147 ± 10	0
${}_0T_{18}$	2553.047 ± 0.35	0.81	143 ± 10	-1
${}_0T_{19}$	2665.755 ± 0.18	1.03	142 ± 10	-1
${}_0T_{20}$	2777.589 ± 0.33	0.90	139 ± 10	-2
${}_0T_{21}$	2888.669 ± 0.45	0.45	133 ± 10	-7
${}_0T_{22}$	3000.254 ± 0.21	0.86	130 ± 10	-9
${}_1S_2$	680.237 ± 0.15	0.38	367 ± 23	57
${}_1S_3$	940.139 ± 0.10	0.31	312 ± 12	30
${}_1S_4$	1172.990 ± 0.05	0.13	295 ± 10	24
${}_1S_5$	1370.150 ± 0.10	-0.12	331 ± 10	39
${}_1S_6$	1521.470 ± 0.10	-0.57	395 ± 12	50
${}_1S_7$	1654.570 ± 0.05	-0.95	425 ± 13	53
${}_1S_8$	1797.930 ± 0.05	-1.38	417 ± 11	38
${}_1S_9$	1961.820 ± 0.05	-1.94	424 ± 14	44
${}_1S_{10}$	2146.020 ± 0.16	-2.43	405 ± 24	26
${}_1S_{14}$	2974.390 ± 1.01	-1.44	284 ± 76	-9
${}_1T_1$	1235.579 ± 0.48	-0.53	268 ± 30	8
${}_1T_2$	1319.245 ± 0.22	-0.86	295 ± 42	38
${}_1T_3$	1438.340 ± 0.22	-0.77	273 ± 33	21
${}_1T_4$	1585.095 ± 0.22	-0.39	290 ± 34	41
${}_1T_5$	1750.133 ± 0.10	-0.36	274 ± 15	28
${}_1T_6$	1925.114 ± 0.10	-0.50	263 ± 10	21
${}_1T_7$	2102.955 ± 0.18	-0.85	284 ± 26	47
${}_1T_8$	2279.491 ± 0.19	-0.76	270 ± 30	38
${}_1T_9$	2452.413 ± 0.23	-0.10	252 ± 13	24
${}_2S_3$	1242.980 ± 0.15	0.79	455 ± 39	39
${}_2S_4$	1379.560 ± 0.10	0.37	388 ± 17	8
${}_2S_5$	1515.370 ± 0.10	0.44	310 ± 17	8
${}_2S_6$	1681.270 ± 0.06	0.43	246 ± 10	8
${}_2S_7$	1865.240 ± 0.23	0.28	214 ± 10	2
${}_2S_8$	2049.650 ± 0.08	0.44	205 ± 10	7
${}_2S_9$	2229.280 ± 0.18	0.53	189 ± 11	1
${}_2S_{10}$	2403.160 ± 0.20	0.23	188 ± 10	7
${}_2S_{11}$	2572.660 ± 0.33	0.51	182 ± 14	6
${}_2S_{12}$	2737.690 ± 0.39	0.38	162 ± 10	-11
${}_2S_{13}$	2899.990 ± 0.20	0.10	165 ± 10	-8
${}_2T_2$	2232.801 ± 0.27	1.99	235 ± 31	30
${}_2T_4$	2379.093 ± 0.15	-0.74	233 ± 18	24
${}_2T_8$	2912.668 ± 0.49	-1.30	279 ± 59	49
${}_3S_1$	944.364 ± 0.10	0.42	906 ± 139	79
${}_3S_2$	1106.480 ± 0.15	0.27	283 ± 10	-82
${}_3S_6$	2548.930 ± 0.32	-0.71	308 ± 31	33
${}_3S_7$	2685.900 ± 0.21	-0.43	275 ± 22	6
${}_3S_8$	2819.300 ± 0.11	-0.34	271 ± 14	8
${}_3S_9$	2950.949 ± 0.11	-0.64	264 ± 13	5
${}_4S_1$	1411.750 ± 0.29	-0.88	365 ± 33	10
${}_4S_2$	1721.580 ± 0.12	-0.72	472 ± 30	37
${}_4S_3$	2048.130 ± 0.05	-0.83	526 ± 27	46
${}_4S_4$	2278.310 ± 0.12	-1.29	308 ± 21	17
${}_4S_5$	2411.180 ± 0.18	-0.25	283 ± 26	0
${}_5S_2$	2090.550 ± 0.15	-0.72	320 ± 10	2
${}_5S_3$	2168.760 ± 0.05	-0.90	320 ± 10	28
${}_5S_4$	2379.250 ± 0.05	-0.27	552 ± 20	63
${}_5S_5$	2703.550 ± 0.06	0.20	570 ± 33	67
${}_5S_6$	3011.380 ± 0.05	0.69	578 ± 22	72
${}_6S_1$	1983.330 ± 0.36	2.95	293 ± 29	-356
${}_6S_3$	2821.860 ± 0.10	0.14	495 ± 27	68
${}_8S_1$	2872.600 ± 0.10	-0.76	999 ± 83	70

[a]Minimum frequency uncertainty is set to 0.05 μHz.
[b]Minimum Q uncertainty is 5 for ${}_0S$ modes and 10 otherwise.

tating aspherical Earth model have frequencies near to the degenerate frequencies of the corresponding SNRAI Earth multiplets, but their eigenfunctions are linear combinations of those of all the SNRAI modes. The expansion coefficients of these linear combinations are components of the eigenvectors of an interaction matrix, $\mathbf{Z}$, with elements:

$$Z^{mm'}_{nn'll'} = D^m_{nn'l}\delta_{ll'}\delta_{mm'} + \sum_{s,t}\Gamma_{ll's}\, c^t_{s(nn'll')}\,. \quad (3)$$

Modal frequencies are determined from the eigenvalues of this matrix. Each element of $\mathbf{Z}$ describes the interaction, or coupling, of a pair of normal modes through aspherical structure. We call coupling of modes within a SNRAI Earth multiplet ($k = k'$) self-coupling, while cross-coupling refers to coupling between modes of different SNRAI multiplets ($k \neq k'$).

The D term of equation (3) includes multiplet degenerate frequency and the effects of multiplet spacing and of the Earth's rotation and ellipticity. The Γ factors are analytic functions that result from the geometry of the spherical harmonic basis functions. These factors multiply structure coefficients of the form

$$c^t_{s(kk')} = \int_0^{r_E} \delta\mathbf{m}^t_s(r)\cdot\mathbf{M}_{s(kk')}(r) r^2 dr + \sum_d h^t_{sd} B_{sd(kk')} r^2_d, \quad (4)$$

with structural kernels, $\mathbf{M}(r) = [K(r), M(r), R(r)]$, and boundary factors, B_d, that are known functions of the radial eigenfunctions of the spherical Earth modes. Structural perturbations and kernels also can be expressed as functions of v_s, v_p, and ρ, as is the case for the kernels shown on Plate 1.

The complex structure coefficients are linear functionals of aspherical structure which summarize the impact of aspherical structure on the modes k and k'. The real and imaginary parts of degree $s = 0$ structure coefficients are related to perturbations to the multiplet degenerate frequency and attenuation, respectively, predicted by the SNRAI reference model and are functions of spherically symmetric elastic and anelastic structures. Under the spherical harmonic normalization we employ, structure coefficients have units of frequency, and $c^{-t}_s = (-1)^t c^{*t}_s$. In several other studies [e.g., He and Tromp, 1996], structure coefficients for self-coupling are reported in the dimensionless form (A^t_s, B^t_s) where $c^t_s = (-1)^t\sqrt{2\pi}\omega^{\text{ref}}(A^t_s - iB^t_s)$ for $t > 0$, $c^t_s = \sqrt{2\pi}\omega^{\text{ref}}(A^{|t|}_s + iB^{|t|}_s)$ for $t < 0$ and $c^0_s = \sqrt{4\pi}\omega^{\text{ref}}A^0_s$. ω^{ref} is multiplet degenerate frequency (in units of mHz or μHz), or the average frequency of a pair of coupled multiplets. The above theory has been presented in full by *Woodhouse and Dahlen* [1978] and *Woodhouse* [1980].

The strength of the impacts of modal couplings on seismic spectra varies inversely with the frequency difference between the singlets. Normal mode spectra, therefore, are often approximated using truncated inter-

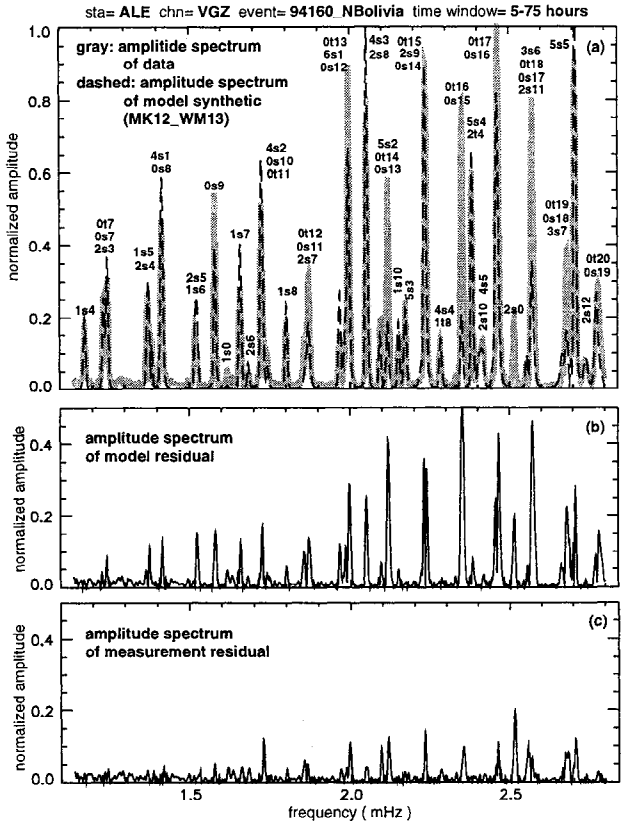

Figure 3. Sample comparisons of low-frequency normal mode spectra of data and synthetic seismograms. (a) Data amplitude spectrum from the IDA station ALE in Alert, Northwest Territories, after the deep Bolivian event of June 6, 1994, and the spectrum predicted by the recent Harvard model MK12_WM13 [*Dziewonski and Su,* 1995]. (b) The amplitude of the difference between these two complex spectra. In this example, which is typical of high signal-to-noise records, many multiplet peaks are misfit by more than 20%. (c) The amplitude of the difference between the data and a synthetic spectrum constructed using the structure coefficients reported here. The largest amplitudes of the residuals in this case are nearer to the 10% level.

action matrices, in which it is assumed that only $k=k'$ terms in equations (3) and (4) are nonzero. This is the multiplet self-coupling approximation, which has been employed in most normal mode studies. More accurate synthetic formalisms employ interaction matrices in which both self-coupling and multiplet cross-coupling ($k \neq k'$) terms are computed for sets of two or more multiplets closely spaced in frequency [e.g., *Masters et al.,* 1983; *Park,* 1986; *Park and Gilbert,* 1986; *Masters,* 1989; *Resovsky and Ritzwoller,* 1994]. Even for multiplets closely spaced in frequency, cross-coupling is not always significant. The strength of coupling depends not only on frequency spacing but also on geometric selection rules and the relative attenuations and sensitivity kernels of the modes involved. In performing GSF on multiplet groups, we employ only those couplings which synthetic experiments show to be significant.

Geometric selection rules, included in the Γ factors of equation (3), determine which aspherical structures can affect modal coupling. For each pair (k, k') of multiplets the structural degrees that can contribute to coupling are confined to $\mid l - l' \mid \leq s \leq (l + l')$. Additionally, for multiplet self-coupling, $\Gamma = 0$ when s is odd, and the structure coefficients depend only on even-degree structures up to $s = 2l$. The use of the self-coupling approximation has confined all previous normal mode studies, with the exception of that of *Resovsky and Ritzwoller* [1995a], to estimates of constraints on only the even degrees of aspherical Earth structure.

For spheroidal-spheroidal or toroidal-toroidal cross-coupling, $k \neq k'$ and $\Gamma = 0$ for $(l+l'+s)$ odd. In the case of the cross-coupling of spheroidal-toroidal multiplet pairs, $\Gamma = 0$ for $(l + l' + s)$ even. For example, nonzero structure coefficients of the overtone pair ${}_1S_5 - {}_2S_4$ exist only for $s = 1, 3, 5, 7, 9$, and those for ${}_4S_4 - {}_1T_8$ are at $s = 5, 7, 9, 11$. Structure coefficient estimates for these types of cross-coupling, which have been obtained only after the introduction of GSF [*Resovsky and Ritzwoller,* 1995a], constitute the only normal mode constraints on odd-degree structures. Cross-coupling structure coefficients can also constrain even-degree structures. For example, coupling coefficients of the multiplet pair ${}_0S_{11} - {}_2S_7$ are nonzero only for even harmonic degrees $s = 4$ through $s = 18$. In the 1.5 to 3.0 mHz range the cross-coupling of fundamental multiplet pairs of the form ${}_0S_l - {}_0T_{(l+1)}$ is relatively strong and is dominantly produced by the Coriolis force.

Using the interaction matrix to describe the modes of an aspherical Earth model, a synthetic seismogram for a receiver at position $\mathbf{r}_R$ is given by

$$s(\mathbf{r}_R, t) = \mathcal{R} \cdot e^{i\mathbf{Z}t} \cdot \mathcal{S} e^{it\omega^{\text{ref}}} , \qquad (5)$$

where, as in the work of *Woodhouse and Girnius* [1982], $\mathcal{R}$ is a receiver vector combining instrument response information with modal displacement eigenfunctions at the receiver, while $\mathcal{S}$ is a product of the moment and strain tensors at the source location. Equation (5) is accurate only to zeroth-order in the eigenfunctions and neglects first-order kinetic energy, Coriolis, and attenuation effects on eigenfunction normalization [*Park and Gilbert,* 1986; *Lognonné,* 1991; F. Dahlen and J. Tromp, *Free Oscillations of the Earth,* text in preparation, 1997]. The effects of this approximation are discussed further in section 3.1.

2.2. Regressions for Structure Coefficients

In GSF, structure coefficients are estimated by linearizing their effect on the data. The spectral residual of record j, produced by estimates of the coefficients after $n-1$ iterations, is $\Delta s_j^{(n)}(\omega_i) = s_j^{\text{data}}(\omega_i) - s_j^{(n-1)}(\omega_i)$ for each discrete frequency (ω_i) in a window including the multiplet group being analyzed. Gaps and edits of the data time series are included in the synthetic time

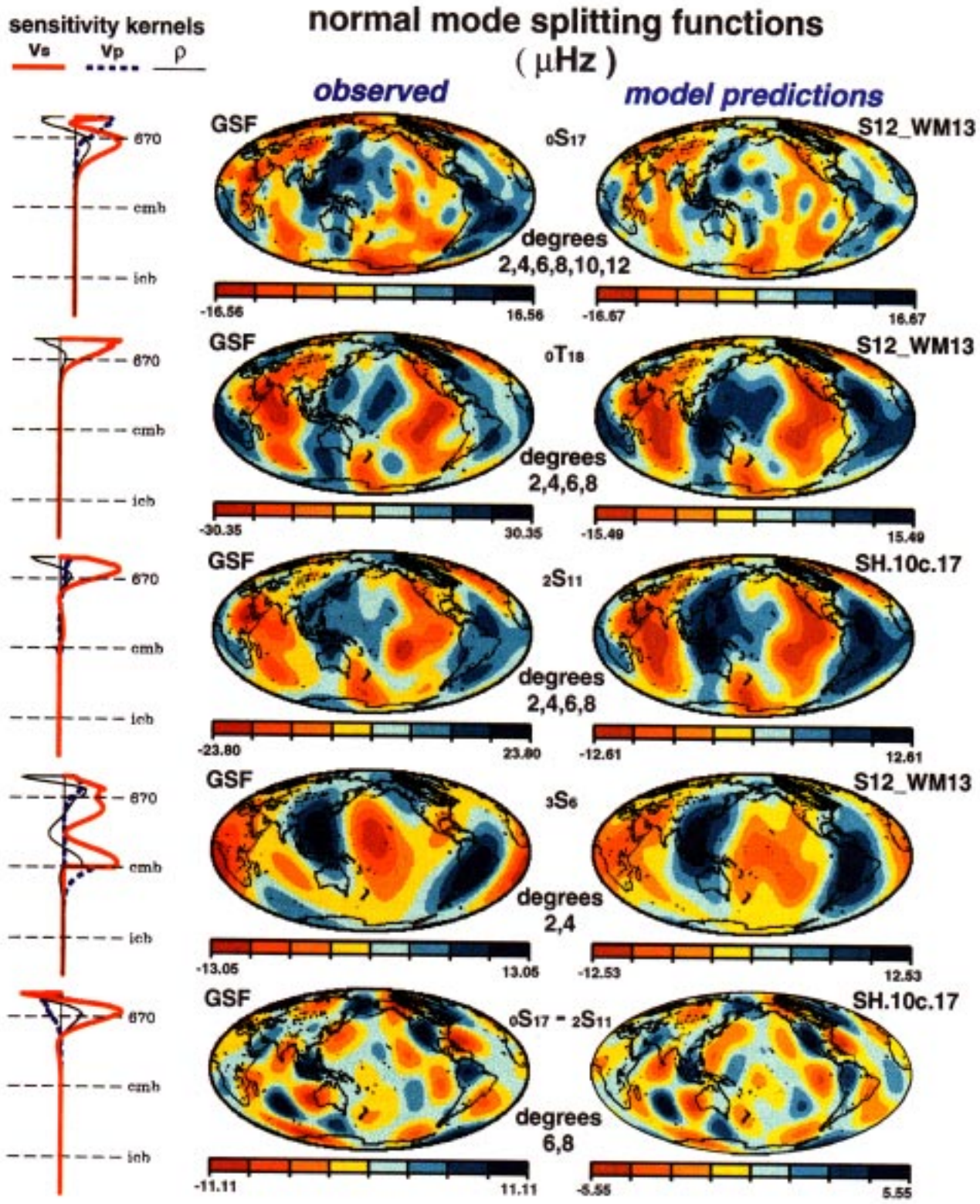

Plate 1. Generalized splitting functions from GSF estimates of self-coupling and cross-coupling structure coefficients. Also displayed are the splitting functions predicted by whichever of mantle models SH.10c.17 or S12_WM13 best agrees with the estimates. To the left are normalized kernels indicating the sensitivities of the multiplets to lateral variations in v_s (thick solid lines), v_p (thick dashed), and density (thin solid) as functions of depth. Note that ${}_0S_3$ exhibits an anomalous splitting function typical of multiplets sensitive to inner-core anisotropy.

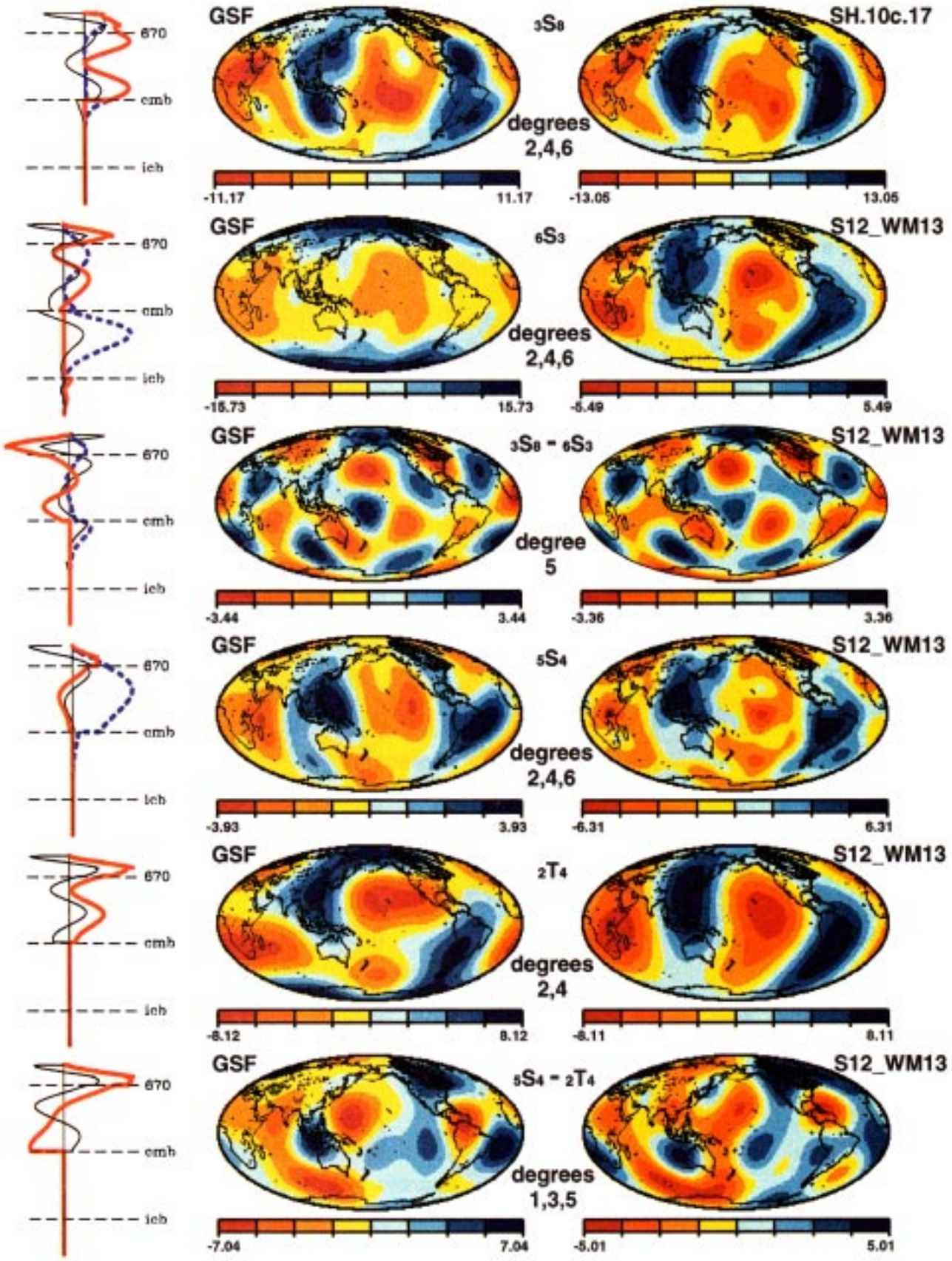

Plate 1. (continued)

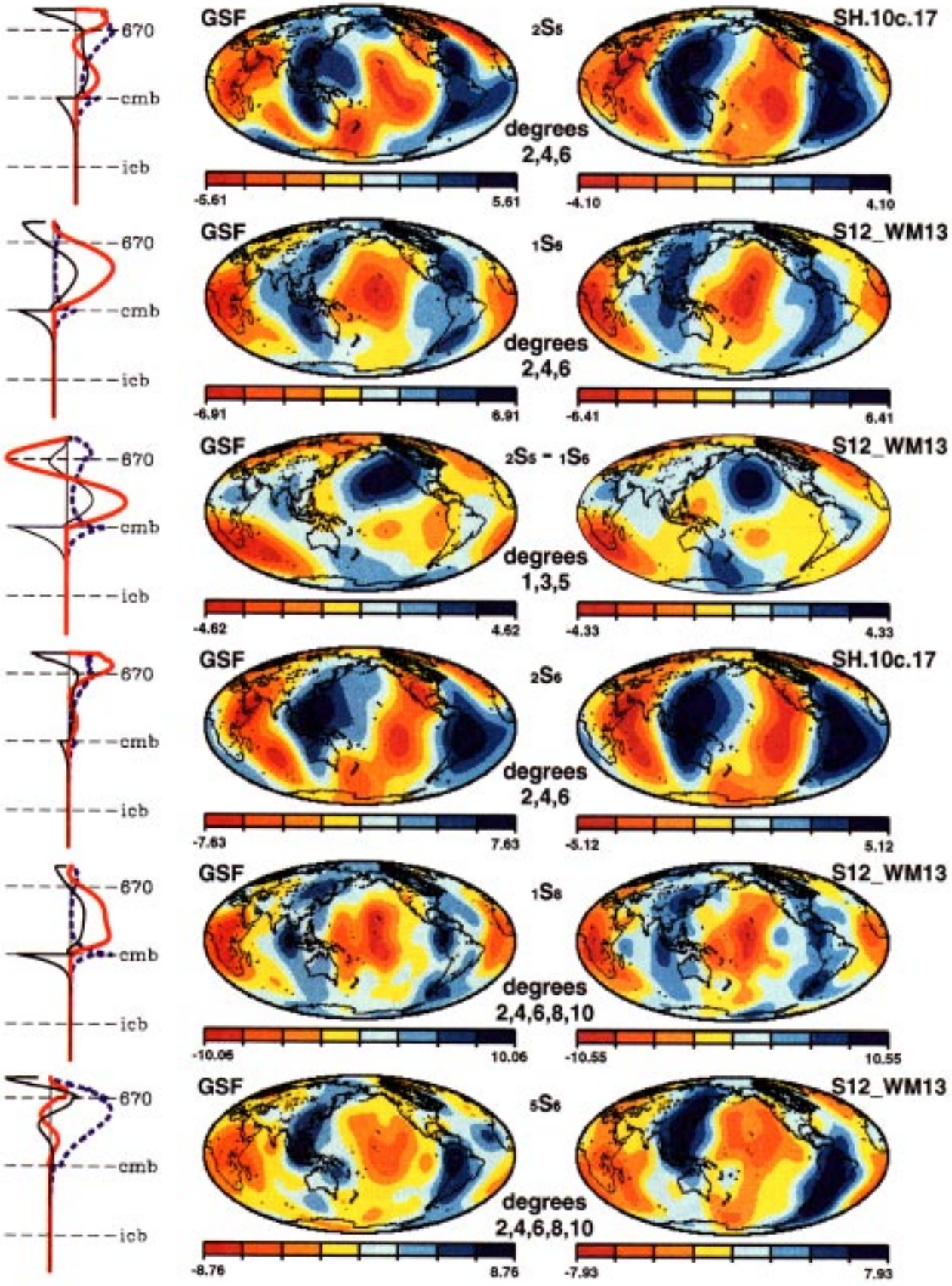

Plate 1. (continued)

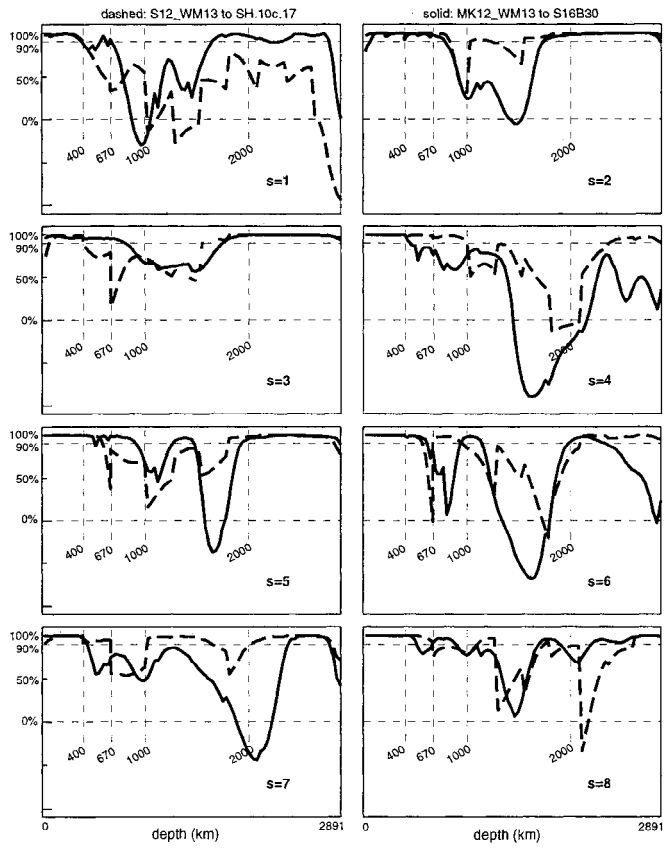

Figure 4. Intermodel correlations for two generations of mantle models expressed in terms of confidence levels (%) [*Eckhardt*, 1984] as functions of depth at structural degrees 1-8. Models S12_WM13 and MK12_WM13 are from Harvard. Models SH.10c.17 and S16B30 are from Scripps Institution of Oceanography. Only the shear velocity components of the models are compared. Correlations between models from the two research groups have remained poor in the mid-mantle and the upper part of the lower mantle.

series before data and synthetics are transformed and compared in the frequency domain.

The structure coefficients of the next iteration are given by $c^{t(n)}_{s(kk')} = c^{t(n-1)}_{s(kk')} + \delta c^{t(n)}_{s(kk')}$, where the perturbations are estimated using the first-order approximation

$$\Delta s_j^{(n)}(\omega_i) = \sum_k \sum_{s,t} \left[\frac{\partial s_j(\omega_i)}{\partial c^t_{s(k)}} \right]^{(n)} \delta c^{t\,(n)}_{s(k)} + \sum_k \sum_{k' \neq k} \sum_{s,t} \left[\frac{\partial s_j(\omega_i)}{\partial c^t_{s(kk')}} \right]^{(n)} \delta c^{t\,(n)}_{s(kk')} . \quad (6)$$

The right side of equation (6) is broken into separate sums over perturbations to the self-coupling and cross-coupling structure coefficients of the multiplets targeted for analysis. The structure coefficients for self-coupling are referred to with a single multipet index k. We compute the partial derivatives of equation (6) with numerical finite differences.

Equation (6) is equivalent to a matrix equation of the form $\Delta \mathbf{s}^{(n)} = \mathbf{A}^{(n)} \cdot \delta \mathbf{c}^{(n)}$. The residual vector, $\Delta \mathbf{s}^{(n)}$, has an element for each frequency of each spectrum, and the perturbation vector, $\delta \mathbf{c}^{(n)}$, has an element for each self-coupling and cross-coupling structure coefficient. $\mathbf{A}^{(n)}$ is the matrix of partial derivatives. In practice, the regressions employ a row weight, w_j, as described in section 3.3. These row weights become the nonzero elements of a diagonal matrix, $\mathbf{W}$, that modifies the matrix equation. With iteration indices now suppressed, equation (6) becomes

$$\mathbf{W} \cdot \Delta \mathbf{s} = \mathbf{W} \cdot \mathbf{A} \cdot \delta \mathbf{c} . \quad (7)$$

$\mathbf{W} \cdot \mathbf{A}$ is referred to as the regression matrix. For each iteration of GSF, the singular value decomposition (SVD) of the regression matrix is used to find the perturbation estimates according to

$$\delta \mathbf{c} = \mathbf{V} \cdot \mathbf{\Lambda}^{-1} \cdot \mathbf{U}^{\mathrm{T}} \cdot \mathbf{W} \cdot \Delta \mathbf{s} . \quad (8)$$

$\mathbf{W} \cdot \mathbf{A}$ is decomposed by the rectangular matrix $\mathbf{U}$, the square matrix $\mathbf{V}$, and the diagonal matrix of singular values, $\Lambda_{pq} = \delta_{pq} \lambda_p$. The stability of the algorithm is enhanced by normalizing the square of the Euclidean norm of each column of $\mathbf{W} \cdot \mathbf{A}$ [*Lawson and Hanson*, 1974]. For a regression to be considered converged, we

have required that the coefficients estimated in the last three successive iterations exhibit convergence through correlation with better than 99% confidence and amplitude differences of less than 2%.

With sufficient data, theoretical errors and noise significantly bias only the amplitudes of coefficients of the highest structural degrees estimated (see section 3). Since it is our practice to specify regressions to higher degrees than we report, the only damping applied in GSF regressions is singular value truncation, which occurs for all singular values λ such that $\lambda_{\max}/\lambda > 20$. Estimates are not reported when truncation is required for more than 5% of the singular values for the specified coefficients. The starting model for most GSF regressions is PREM [*Dziewonski and Anderson,* 1981]. With the truncation and weighting that we use, the regressions usually converge within a dozen iterations. Regressions which use the predictions of various aspherical models as initial structure coefficient estimates generally converge to the same final estimates within the reported uncertainties. In the frequency band we consider, regressions for the anomalous multiplet ${}_3S_2$ are the only exception to this rule.

GSF regressions provide structure coefficient estimates for each targeted self-coupled multiplet and cross-coupled multiplet pair. These coefficients may be displayed in map form using generalized splitting functions:

$$F_{kk'}(\theta,\phi) = \sum_{s,t} c^t_{s(kk')} Y^t_s(\theta,\phi) \,. \qquad (9)$$

This is a generalization of the self-coupling splitting functions defined by *Giardini et al.* [1987]. These functions, which have units of frequency (μHz), are the normal mode analogue of surface wave phase velocity maps and display the structure of the Earth under each point, averaged by the depth sensitivity kernels of the multiplets in question. Plate 1 displays several estimated splitting functions.

2.3. New Capabilities of GSF

By incorporating the effects of cross-coupling, GSF improves on traditional spectral fitting by yielding better fits to normal mode spectra, more accurate structure coefficient estimates, and estimates of several new types of structure coefficients. Many normal mode multiplets appear in clusters such as the group ${}_3S_6$-${}_0T_{18}$-${}_0S_{17}$-${}_2S_{11}$. Figure 5a shows that each of these multiplets is noticeably expressed in the data and that the overtones underlie the fundamentals. Figure 5b demonstrates the spectral signatures of the Coriolis coupling between ${}_0T_{18}$ and ${}_0S_{17}$, the coupling of this pair through (even-degree) aspherical structure, and the structural coupling between ${}_0S_{17}$ and ${}_2S_{11}$. Each effect is significant, especially relative to the strength of the overtone signals suggested by Figure 5a, and the inclusion of each improves the fit to the data.

Cross-coupling also has a significant effect on structure coefficient estimates. Figure 6 illustrates the results of a synthetic experiment in which spectral fitting without coupling is applied to synthetic spectra which incorporate Coriolis coupling. The impact of Coriolis coupling on estimates of degenerate frequency, Q, and $t = 0$ (zonal) coefficients can be approximated [*Smith and Masters,* 1989a,b], but as Figure 6 demonstrates,

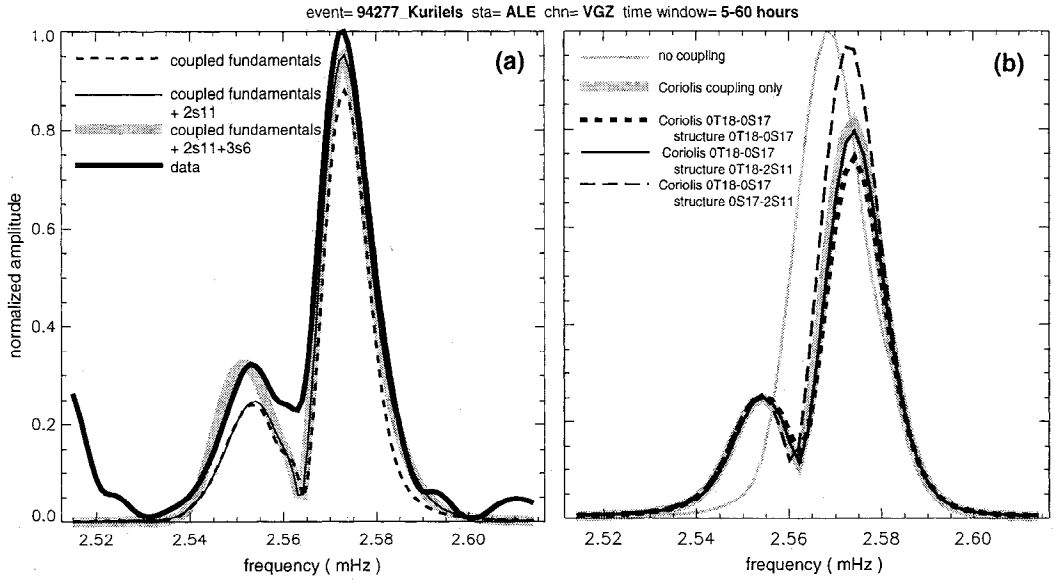

Figure 5. (a) Sample spectra illustrating the effect of the presence of overtones beneath a pair of fundamental multiplet peaks. The synthetic spectra are constructed using GSF estimates of structure coefficients. The time window here is intermediate between those which best accentuate the individual multiplets. (b) Sample spectra illustrating the relative impacts of the various couplings of ${}_0T_{18}$-${}_0S_{17}$-${}_2S_{11}$.

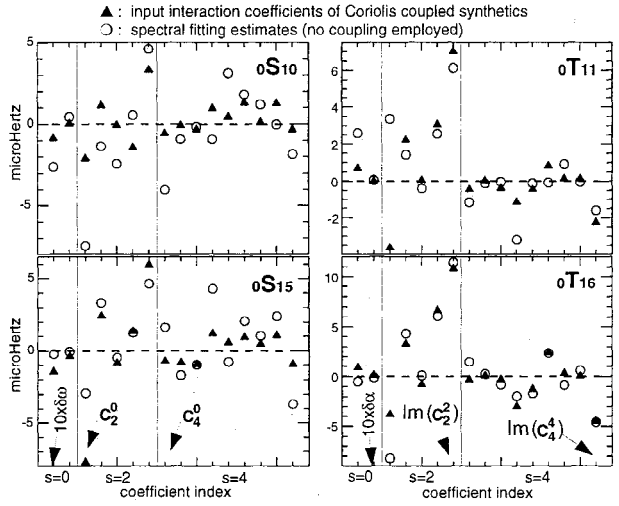

Figure 6. Input and estimated structure coefficients for a synthetic experiment. Input synthetics incorporate Coriolis cross-coupling of $_0S_{10}$-$_0T_{11}$ and $_0T_{16}$-$_0S_{15}$, while output estimates are made with regressions that do not incorporate cross-coupling. The plotted coefficients are ordered, left-to-right, $(10 \times \delta\omega)$, $(10 \times \delta\alpha)$, c_2^0, Re(c_2^1), Im(c_2^1), Re(c_2^2), Im(c_2^2), c_4^0, ..., Im(c_4^4). Inputs and outputs differ as much for several nonzonal coefficients (azimuthal order $t \neq 0$) as they do for frequency, attenuation, and $t = 0$ coefficients.

failure to include Coriolis coupling in spectral fitting regressions which fit amplitude and phase simultaneously can also produce significant bias in nonzonal coefficients for strongly coupled fundamentals [*Resovsky and Ritzwoller,* 1995b]. Cross-coupling through aspherical structure produces similar effects.

In general, we observe that the incorporation of significant couplings improves the internal consistency of structure coefficient estimates for similar multiplets, and agreement, or external consistency, between estimates and the predictions of reliable models. This behavior is demonstrated in Table 3 and Table 4, using estimates of $_0T_{18}$, $_0S_{17}$, and $_2S_{11}$ self-coupling structure coefficients made with four regressions: (Trial 1) without coupling; (Trial 2) with only Coriolis coupling; (Trial 3) with Coriolis coupling and specified structural coupling between $_0S_{17}$ and $_2S_{11}$; and (Trial 4) with these couplings plus specified structural coupling between $_0T_{18}$ and $_0S_{17}$. These trials are performed using the same data set employed in our final GSF regressions for these multiplets.

Table 3 displays internal consistency using lateral correlations of the estimated $_0T_{18}$, $_0S_{17}$, and $_2S_{11}$ splitting functions with those for adjacent multiplets of the respective mode branches: $_0T_{17}$ and $_0T_{19}$, $_0S_{16}$ and $_0S_{18}$, $_2S_{10}$, and $_2S_{12}$. The incorporation of each additional form of coupling improves the overall "along-branch" correlation for each of the three multiplets and usually improves correlation at each individual spherical harmonic degree for each multiplet. Table 4 compares the estimated structure coefficients to predictions of model SH.10c.17, using splitting function difference ratios which are the amplitude of the difference of estimated and predicted splitting functions, divided by the amplitude of the model splitting functions. Overall difference between our estimated splitting functions and those predicted by model SH.10c.17, as well as differences at most individual harmonic degrees for each splitting function, are smaller for regressions which incorporate more coupling.

In earlier spectral fitting studies, only the first term on the right of equation (6) was employed in the regressions, so that only the self-coupling ($k' = k$) structure coefficients were estimated. This approximation yielded constraints on only even-degree aspherical structures. GSF estimates of cross-coupling structure coefficients provide the first normal mode constraints on odd-degree aspherical structures. Plate 1 includes examples of estimated odd-degree splitting functions. Both odd- and even-degree cross-coupling coefficients possess unique depth dependencies, since the integral kernels for a cross-coupled multiplet pair are hybrids of those for the self-coupling of the individual multiplets in the pair. Plate 1 displays plots of such hybridized kernels for $_0S_{17}$-$_2S_{11}$, $_3S_8$-$_6S_3$, $_5S_4$-$_2T_4$, and $_2S_5$-$_1S_6$.

We have shown that the incorporation of multiplet cross-coupling is essential to refining structure coefficient estimates for Coriolis-coupled fundamental mode multiplets between 1.5 and 3 mHz. These multiplets are well excited and overlap most overtone multiplets within the 1.5-3 mHz spectral band. For this reason, accurate estimates of structure coefficients, particularly those above degree 4, for most overtones in this band

Table 3. Cross-Coupling and Internal Consistency

		Along-Branch Correlation[a] %			
Modes	Degree	Trial 1[b]	Trial 2	Trial 3	Trial 4
$_0T_{18}$	2	99.0	99.5	99.0	99.1
	4	83.0	76.4	86.9	78.7
	6	78.7	78.2	82.4	85.7
	8	49.4	61.1	65.4	72.7
	all	83.0	84.4	87.5	87.8
$_0S_{17}$	2	97.6	99.8	99.8	99.8
	4	93.7	95.7	95.3	93.9
	6	80.5	90.0	91.9	92.6
	8	73.2	80.5	84.6	84.5
	10	72.4	78.1	78.2	78.9
	12	55.7	64.4	74.9	75.9
	all	88.6	92.6	94.2	94.5
$_2S_{11}$	2	96.1	98.7	99.0	99.0
	4	86.3	81.4	87.4	89.7
	6	74.3	80.0	86.8	85.4
	8	40.6	53.3	57.5	55.6
	all	81.0	85.0	88.3	89.2

[a]Average of correlations with two adjacent multiplets.
[b]Trial regression index, see section 2.3.

Table 4. Cross-Coupling and External Consistency

Modes	Degree	Regression Estimates Versus Model[a] Difference Ratios[b]			
		Trial 1[c]	Trial 2	Trial 3	Trial 4
${}_0T_{18}$	2	0.42	0.49	0.47	0.49
	4	0.81	0.74	0.54	0.79
	6	1.52	1.41	1.44	1.13
	8	2.45	1.93	2.13	2.16
	all	0.88	0.82	0.81	0.78
${}_0S_{17}$	2	0.32	0.16	0.19	0.18
	4	1.23	0.84	0.83	0.79
	6	1.62	1.38	1.35	1.20
	8	1.82	1.32	1.19	1.23
	all	0.61	0.44	0.43	0.41
${}_2S_{11}$	2	0.49	0.40	0.37	0.27
	4	0.50	0.89	0.66	0.70
	6	1.99	1.38	1.33	1.33
	8	2.58	2.46	2.22	1.70
	all	0.95	0.82	0.74	0.66

[a]Predictions from model SH.10c.17.
[b] [RMS (estimated-model)]/[RMS model].
[c]Regression index, see section 2.3.

can be obtained only if the signal of the fundamental modes is well fit. With GSF, we have retrieved the first structure coefficient estimates for several overtone multiplets (e.g., ${}_2S_7$, ${}_2S_9$, ${}_2S_{11}$, ${}_3S_6$, ${}_3S_7$, ${}_6S_1$, and ${}_8S_1$) and have extended and refined sets of coefficient estimates for other overtones.

GSF may also be employed in the simultaneous estimation of structure coefficients and corrections to source parameters. As discussed in section 3.1.3, this capability has been used to obtain new moment estimates for the largest events in our data set. GSF has the additional, as yet unexploited, capability to estimate the structure coefficients for aspherical anelastic structure.

3. Issues of Precision and Accuracy

Spectral fitting has been generalized not only to extend the capabilities of the analysis of normal mode data but also to insure that structure coefficient estimates are accurate and precise enough to be used in refining 3-D Earth models. Certain theoretical errors, covariances in regression matrices, and seismic noise produce biases and uncertainties in GSF estimates. We have sought to reduce some of the most significant sources of error, to reduce covariances, and to improve signal-to-noise ratios (SNR). Our coefficient assessments (section 4.3) and error analyses (section 5) attempt to describe and quantify the remaining inaccuracies and imprecision.

3.1. Reducing Theoretical Error

Theoretical errors result from the use of inaccurate synthetic formulations, the effects of structures unspecified in the regressions, and errors in source and receiver information. Of these, errors from unspecified structures are particularly important because there are insufficient data to permit stable regressions for the structure coefficients of all the structures to which the modes in most multiplet groups are sensitive.

3.1.1. Cross-coupling effects. The incorporation of cross-coupling in GSF has allowed us to reduce errors, such as those shown in Figure 6, that can be introduced by Coriolis coupling. The experiments which are documented in Tables 3 and 4 have shown that GSF also reduces theoretical errors caused by unspecified cross-coupling through aspherical structure. This improvement is particularly important when it is caused by structures at the lower degrees ($s = 1$ through 6) that are expected to dominate the spectrum of mantle heterogeneity [*Su and Dziewonski*, 1991]. Examples include degrees 1, 3, and 5 coupling of ${}_5S_4$-${}_2T_4$ and degrees 2, 4, and 6 coupling of ${}_0S_{11}$-${}_0T_{12}$.

3.1.2. Unspecified degrees of structure. In performing GSF, we also seek to reduce theoretical errors resulting from unspecified structures, particularly structures of degrees higher than those specified. Table 5 demonstrates the impact of such structures. In this synthetic experiment the "input" data are synthesized using the self- and cross-coupling structure coefficients through degree 36 for ${}_0T_{18}$, ${}_0S_{17}$, and ${}_2S_{11}$ from a test model. This model consists of degrees 1-16 of S16B30 and a threefold to tenfold amplification of degrees 17-36 structure from model RG5.5 of *Zhang and Tanimoto* [1991]. The source and receiver distribution in the synthetic data is the same as for regressions performed on real data for these multiplets. GSF is

Table 5. Effects of Higher Degree Unspecified Structure

Modes	Degree	Estimated Splitting Functions Versus Inputs	
		Correlation, %	RMS Ratio[a]
${}_0T_{18}$	2	99.84	0.952
	4	98.23	0.918
	6	98.02	1.095
	8	78.48	0.966
	10	74.39	1.638
${}_0S_{17}$	2	99.97	1.009
	4	98.77	1.106
	6	96.62	1.070
	8	92.88	1.215
	10	89.55	1.034
	12	81.06	1.276
	14	50.56	2.034
${}_2S_{11}$	2	99.96	1.087
	4	95.55	0.996
	6	86.68	1.113
	8	84.87	1.264
${}_0S_{17}$-${}_2S_{11}$	6	98.73	0.973
	8	94.08	1.180

[a] [RMS amplitude estimated]/[RMS amplitude input].

applied to the synthetic data, with only the tabulated degrees specified, to obtain the output coefficient estimates. The comparisons of Table 5 show that both the geometry and the amplitude of estimated splitting functions can be appreciably affected by unspecified higher degree structure. This effect results from the coefficient covariances inherent in GSF, as discussed in the following subsections, and is dominately manifested in the highest degree structure coefficients estimated for each multiplet and coupling pair.

Therefore, to reduce errors from unspecified higher-degree structures, we specify regressions to the highest degrees possible. In particular, we specify coefficients for structures of degrees higher than those we report. If we report coefficients through degree 10, regressions have been specified at least to degree 12 and preferably to degree 14 for that multiplet. Exceptions occur for fully specified multiplets such as ${}_4S_3$, which is sensitive only to degrees 0-6, or for multiplets such as ${}_0S_4$ which are only weakly sensitive to aspherical structure.

3.1.3. Source and receiver errors. We account for some of the theoretical error introduced by incorrect source solutions by using GSF to estimate source moments for the largest events used. These estimates are plotted in Figure 7. Future applications of GSF may specify other source parameters. Errors in reported instrument responses are generally difficult to identify, but we are able to find and correct sign errors and discard data with anomalous amplitudes.

3.1.4. Other theoretical errors. Among other potential sources of theoretical error in the present form of GSF are first-order corrections to eigenfunction normalization [e.g., *Lognonné,* 1991], aspherical anelastic structures [*Resovsky and Ritzwoller,* 1992, 1994], and aspherical anisotropy. The size and relative importance of these effects, as well as those of source and receiver errors, may vary greatly from multiplet to multiplet. We are currently modeling some of these variations in order to inform future modifications of the GSF method.

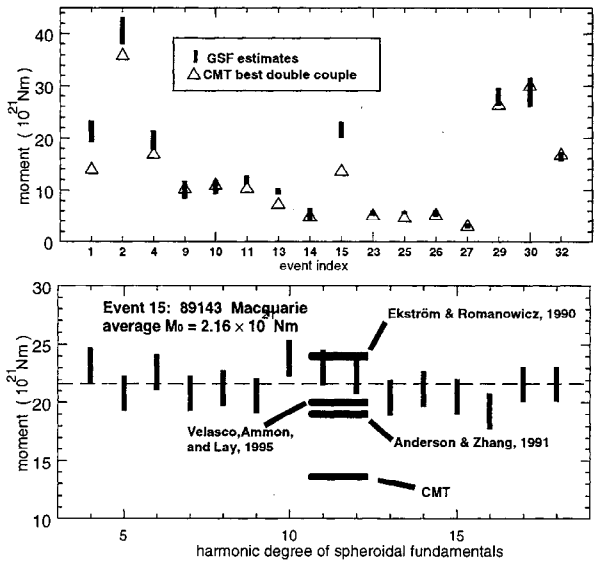

Figure 7. (top) Moment estimates from generalized spectral fitting. Event indices refer to Table 1. The moment estimate for each event is the average of the results from regressions for multiplet groups for which at least 10 recordings from that event were employed. (bottom) Moment estimates for the 1989 Macquarie Ridge event made using ${}_0S$ branch multiplet peaks.

3.2. Reducing Covariances

The number of distinct seismograms employed in GSF is important in determining the number of structure coefficients that can be retrieved and reported with reasonable confidence. The signal in each seismogram is determined by the source and receiver vectors of equation (5). For a multiplet of degree ℓ, all of the information about the Earth from a single event is contained in the $2\ell+1$ time series $e^{i\mathbf{Z}t}\cdot\mathcal{S}$. Irrespective of how many receivers sample these time series, $2\ell+1$ time series are inadequate to determine much about the structure of the Earth, for realistic signal-to-noise levels. Thus the retrieval of information about structural degrees above $s=4$ usually requires the use of a multiplicity of events, each contributing $2\ell+1$ time series. Normal mode investigations which employ data from only one or two strong events can usually obtain reliable estimates for only even degree structure coefficients through degree 6 at most, as demonstrated by *He and Tromp* [1996].

The covariance matrices that result from GSF demonstrate the advantages of using data from dozens of large events. When SVD is employed, the estimated covariance matrix is

$$C_{ij} = \sum_p \frac{1}{\lambda_p^2} V_{ip} V_{jp}\,, \tag{10}$$

where V_{ij} and λ_i are defined by equation (8) and the diagonal elements of $\mathbf{C}$ provide estimates of the coefficient variances. Because the covariance matrix of equation (10) does not account for covariances with unspecified structures and other theoretical errors, the standard estimates of variance and covariance from equation (10) have repeatedly proven to be inadequate for explaining the observed inconsistencies in normal mode observations [e.g., *Ritzwoller et al.,* 1988]. However, the estimated covariance matrix is a useful tool for understanding certain aspects of inaccuracy and imprecision in GSF estimates. A reliable regression will exhibit a covariance matrix which is approximately diagonal, indicating that structure coefficient estimates are nearly independent; small coefficient variances, indicating that the corresponding structures are well-sampled by the data; and a low matrix condition number, indicating that the coefficient estimates are stable. Matrix condition number is defined as the ratio of the largest to the smallest singular value.

We have examined the properties of covariance matrices for two sequences of trial regressions with data sets comprising increasing numbers of records and events.

These regressions target the isolated multiplet ${}_1S_8$ and the group of coupled multiplets ${}_0T_{18}$-${}_0S_{17}$-${}_2S_{11}$. The ${}_1S_8$ regressions estimate the 92 structure coefficients of even degrees 0-12. The ${}_0T_{18}$-${}_0S_{17}$-${}_2S_{11}$ regressions estimate 264 even degree coefficients for self- and cross-coupling. Figure 8a is a plot of matrix condition number for these regressions. Using the event numbering of Table 1, we indicate which events supply the additional records for each regression in the two sequences. The first several events included are those which provide the largest quantity of high SNR recordings: event 15, Macquarie Ridge, 5/23/89; event 29, Northern Bolivia, 6/9/94; event 30, Kurile Islands, 10/4/94; event 32, Northern Chile, 7/30/95. The inclusion of new events

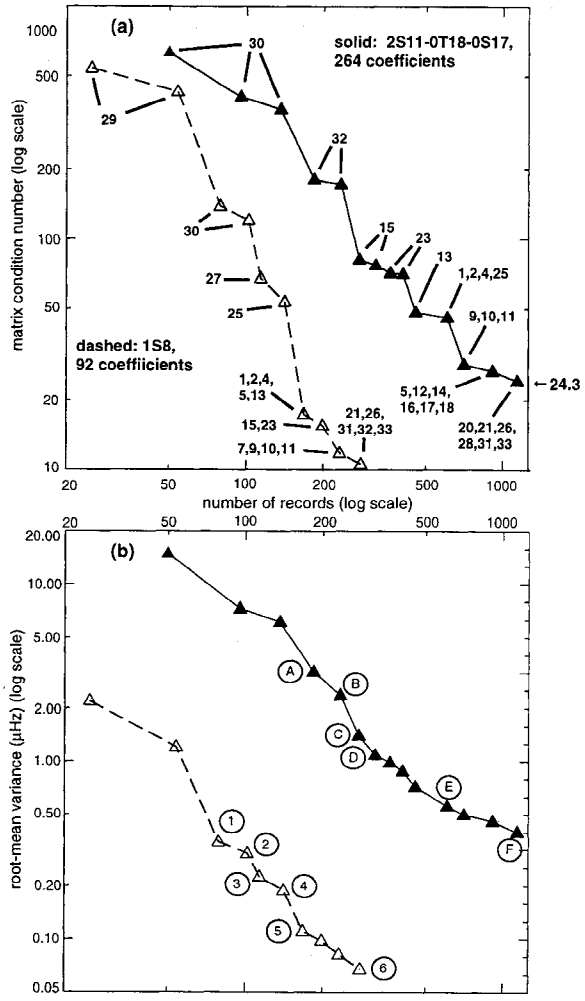

Figure 8. (a) Matrix condition numbers of the singular value decompositions of GSF for a series of regressions employing increasing numbers of stations and events to estimate structure coefficients of ${}_1S_8$ and of ${}_0T_{18}$-${}_0S_{17}$-${}_2S_{11}$. The horizontal axis gives the number of records used and the labels indicate the events which provide each set of additional records. Event numbers refer to Table 1. (b) Root-mean-variances for each of these regressions. The circled numbers and letters mark regressions selected for the plots of Figure 9.

is consistently more effective at improving matrix condition than is the addition of new records from events already included. The condition number associated with regressions employing a dozen or more events can be as much as an order of magnitude less than that for regressions using only the largest two or three events. In Figure 8b, similar behavior is observed for "root-mean-variance", a summary of the estimated coefficient variances defined by $\bar{\sigma} = \sqrt{\sum_j C_{jj}/J}$, where J is the number of specified structure coefficients.

In Figure 8b, we use the numbers 1-6 to mark six ${}_1S_8$ regressions for which we examine covariances with Figure 9a, and letters A-F to indicate the six ${}_0T_{18}$-${}_0S_{17}$-${}_2S_{11}$ regressions with covariances displayed in Figure 9b. The quantity plotted in Figure 9 for each specified coefficient is "root-mean-covariance", defined by $\bar{\sigma}_j = \sqrt{\sum_{i \neq j} C_{ij}/(J-1)}$. Increasing the number of events consistently reduces covariances more effectively than simply including more seismograms in the regressions. Again, nearly order-of-magnitude reductions can be achieved. At the same time, and just as significantly, the addition of events yields increasingly diagonally dominated covariance matrices. This is illustrated by Figure 10, where we use a gray-scale to plot elements of normalized covariance matrices, $\mathbf{C}'$, defined by

$$C'_{ij} = \frac{C_{ij}}{(C_{ii}C_{jj})^{1/2}}. \tag{11}$$

In addition to the effect of using diverse sources, Figure 10 illustrates two other important characteristics of the estimated covariance matrices. First, with data from only three large events, there is considerable covariance among all estimated self-coupling coefficients for ${}_1S_8$. This implies that for ${}_1S_8$ and similar multiplets, the results of using limited data to estimate degrees 0-4 or 0-6 can be significantly biased by unconstrained structures at higher degrees, especially the degrees 8-12 structures that our expanded data set now permits us to specify. The inclusion of data from many events is therefore essential for minimizing the impact of theoretical errors from unspecified higher-degree structures, whether few or many coefficients are specified. This has been confirmed by several experiments [*Ritzwoller and Resovsky,* 1995a].

Second, even when a large number of events are employed, several significant covariances remain. The banded features evident in Figures 10c and 10f indicate three dominant types of persistent covariances: (1) covariances between coefficients of the same multiplet and harmonic degree (s) with azimuthal orders t and t' differing by 2; (2) covariances between coefficients of the same multiplet with s and s' differing by 2 or 4; and (3) covariances between coefficients with identical structural indices ($(s,t)=(s',t')$) from a pair of Coriolis-coupled multiplets. These covariances motivate further expansion of the data set but may be ultimately irre-

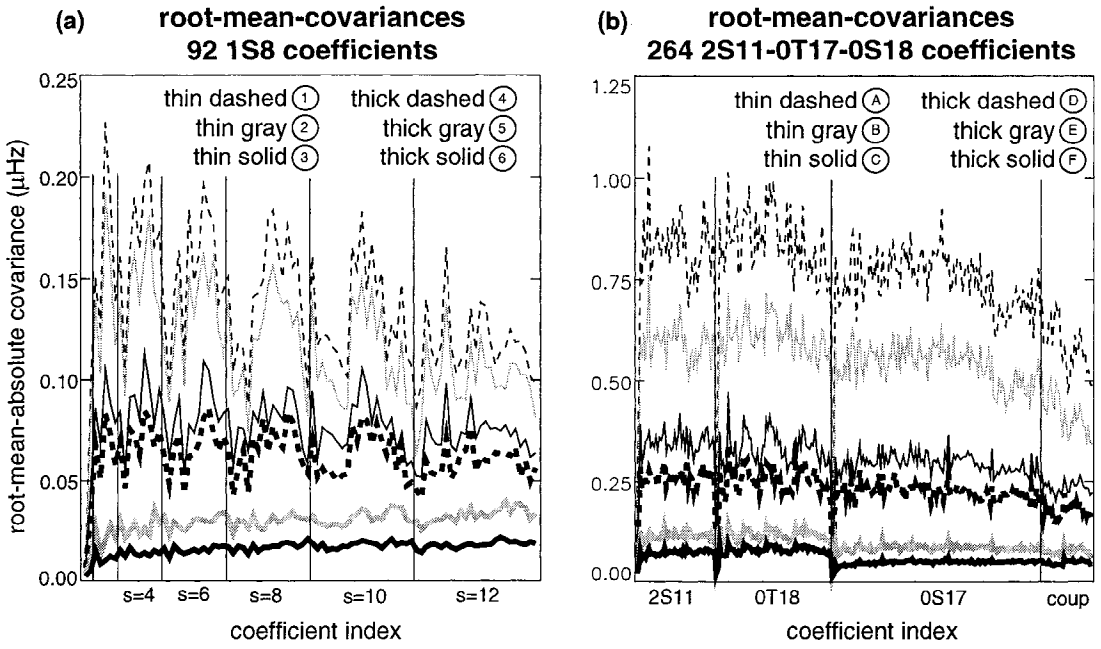

Figure 9. Root-mean-covariances, as functions of variable index, for several of the regressions of Figure 8 for (a) ${}_1S_8$ and (b) ${}_0T_{18}$-${}_0S_{17}$-${}_2S_{11}$. The multiplets are ordered as indicated, with coefficients ordered as in Figure 6.

ducible, indicating that the distributions of large earthquakes and current seismographic stations are not adequate to resolve trade-offs between estimates of the covarying coefficients. It should be noted that the second type of persistent covariance confirms our observation that errors caused by unspecified higher-degree structures are largely confined to the highest degrees specified, as described in section 3.1.2.

3.3. Reducing Noise and Weighting Data

Many of the long-duration seismograms we employ are contaminated by strong tidal signals, large glitches, events near to individual stations, and daily calibration pulses. In assembling the data, we routinely remove tidal signals, by fitting tidal amplitudes at known tidal frequencies, and edit out other contaminating signals. This processing can greatly improve the signal-to-noise ratio in the data, as demonstrated by Figure 11. Considerable "random" seismic noise can remain, especially on recordings from horizontally oriented instruments. For each multiplet, several stations are near nodes of the oscillation pattern, so that modal amplitudes are near the ambient noise levels. For this reason, in addition to detiding and editing all data, we cull the data for each multiplet group by visually inspecting the appropriate spectral window of each seismogram and discarding low SNR records.

Convergence of GSF regressions is enhanced and precision is improved by using a modified form of the weighting (equation (7)) employed by *Ritzwoller et al.* [1988]. For each seismogram (index j) and for the spectral window about a given multiplet group, the RMS residual after each GSF iteration is $\sqrt{v_j}$, where $v_j = [\sum_{i=1}^{I} (\Delta s_j(\omega_i))^2/I]$ is the variance of the residual. The diagonal elements of the weighting matrix $\mathbf{W}$ are

$$w_j = f_j^{\beta}/\sqrt{v_j}, \tag{12}$$

where $f_j = 1 - [v_j/\sum_i s^2_{\mathbf{data}}(\omega_i)]^{1/2}$ is the fractional RMS misfit and values for β range from 0.25 to 2.0. In order to avoid assigning excessively high weights to extremely high SNR records from recent large events, we cap the weights at some small factor (≤ 5) of the median of $1/\sqrt{v_j}$.

4. Results of GSF

4.1. Summary of the Regressions

We have analyzed a total of 90 multiplets below 3 mHz of which 59 are spheroidal and 31 are toroidal. These multiplets and the maximum degree of the structure coefficients reported are indicated in Figure 2. In addition, we have been able to estimate and report structure coefficients for the structural coupling of 25 multiplet pairs. These include degree 1, 3, and 5 coefficients from ${}_1S_5$-${}_2S_4$, ${}_2S_5$-${}_1S_6$, and ${}_5S_4$-${}_2T_4$; degree 5 coefficients from ${}_2S_9$-${}_0S_{14}$, ${}_2S_{10}$-${}_4S_5$, ${}_3S_8$-${}_6S_3$, and ${}_4S_4$-${}_2T_8$; degree 2 coefficients from ${}_1S_3$-${}_3S_1$, ${}_3S_7$-${}_5S_5$, and ${}_0S_{10}$-${}_0T_{11}$ through ${}_0S_{20}$-${}_0T_{21}$; degree 4 coefficients from ${}_1S_3$-${}_3S_1$, and ${}_0S_{11}$-${}_2S_7$; and degree 6 coefficients from ${}_0T_{12}$-${}_2S_7$, ${}_0S_{11}$-${}_2S_7$ and ${}_0S_{17}$-${}_2S_{11}$.

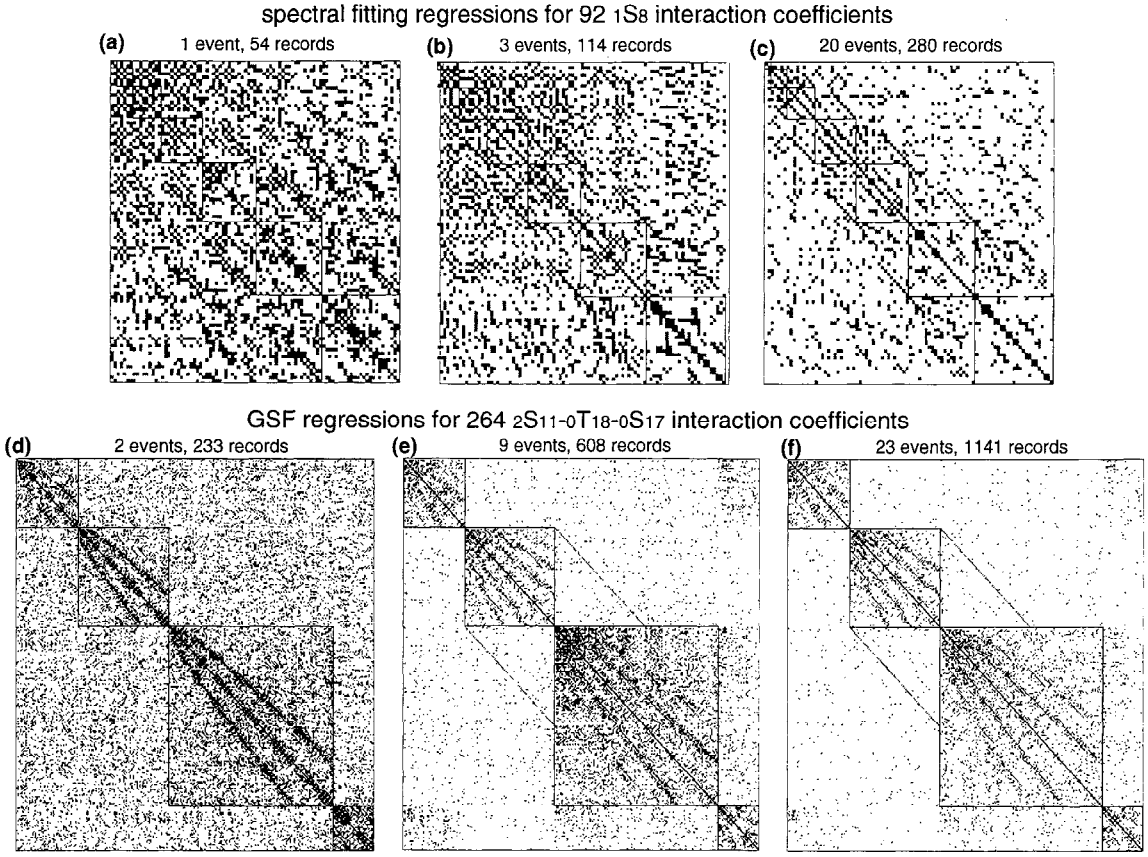

Figure 10. The normalized covariance matrices for several of the regressions of the sequence shown in Figure 8. The darker boxes indicate matrix elements with larger amplitudes. (a)-(c) Even degrees 0-12 structure coefficients of ${}_1S_8$, ordered left-to-right and top-to-bottom starting with real and imaginary parts of degree 0. (d)-(f) Covariances for the self-coupling of ${}_2S_{11}$ are in the top left, followed, moving toward the lower right, by those for ${}_0T_{18}$ and ${}_0S_{17}$, as in Figures 10a-10c. Covariances among the cross-coupling coefficients of ${}_0S_{17}$-${}_2S_{11}$ are in the bottom right corner.

Plate 1 displays a sampling of the generalized splitting function maps that result from our coefficient estimates. For comparison, each splitting function is displayed with a prediction from one of two models, SH.10c.17 or S12_WM13. Plate 1 demonstrates several notable features of the new catalogue. Splitting functions retrieved for multiplets with similar sensitivities to Earth structures, like ${}_0T_{18}$ and ${}_2S_{11}$, are well correlated geographically. Splitting functions estimated through degrees 8, 10, or 12, including those of ${}_0S_{17}$ and ${}_1S_8$, show good correlation with model predictions. This is also true of splitting functions for cross-coupling, including those of low odd degrees (${}_2S_5$-${}_1S_6$), those of higher even degrees (${}_0S_{17}$-${}_2S_{11}$), those from the coupling of spheroidal and toroidal overtones (${}_5S_4$-${}_2T_4$), and those from the coupling of mantle- and core-sensitive multiplets (${}_3S_8$-${}_6S_3$). Estimated splitting functions for multiplets sensitive to shear velocity in the transition zone, like ${}_0S_{17}$, ${}_0T_{18}$, and ${}_2S_{11}$, consistently display larger amplitudes at degrees 6 and 8 than do model predictions. Splitting functions for multiplets sensitive to shear velocity in the core display the familiar, highly axisymmetric signal of inner-core anisotropy [e.g., *Woodhouse et al.*, 1986; *Tromp*, 1993, 1995; *Um et al.*, 1994], which does not appear in the mantle model predictions. The catalogue of new structure coefficient estimates and the associated uncertainties is available as an electronic supplement.[1] At present, the catalogue, together with the splitting function maps, sensitivity kernels, normalization information, and other relevant material, is available at internet site abdu.colorado.edu/geophysics/nm.dir/nm.html.

Seventy-seven regressions were performed to obtain these estimates. For these regressions, Table 6 lists the multiplets and coupling pairs targeted, together with the highest structural degree specified for each. It also documents the total number of specified coefficients, the quantity of events and recordings employed, and

[1]Measurements and related information may be obtained on diskette or via Anonymous FTP from kosmos.agu.org, directory APEND (Username=anonymous, Password=guest). Diskette may be ordered from American Geophysical Union, 2000 Florida Avenue, N. W., Washington, DC 20009 or by phone at 800-966-2481; $15.00. Payment must accompany order.

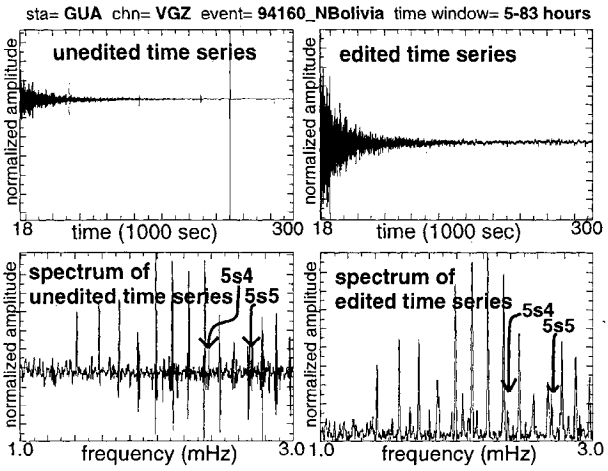

Figure 11. Example of editing to produce reliable data. The large glitches in the original time series produce a large offset and considerable noise in the spectrum. When these are removed by editing, overtone peaks such as the lower mantle ${}_5S$ multiplets become observable.

nearby multiplets included in the regression synthetics. Note that 13 of the regressions specify spheroidal-toroidal pairs coupled through the Coriolis force (${}_0S_9$-${}_0T_{10}$ through ${}_0S_{21}$-${}_0T_{22}$) and that these multiplets are included in another 11 regressions.

4.2. Signal-to-Noise and Misfit

The most import characteristic of GSF regressions, aside from the nature of the structure coefficient estimates that result, is the extent to which they reduce that portion of the misfit between synthetic seismograms and the data not attributable to seismic noise. The average signal-to-noise ratio (SNR) in the data set we employ is typically in the 10:1 to 20:1 range, which is commensurate with the expected size of misfits resulting from theoretical error. However, theoretical errors are expected to manifest as perturbations to modal peaks, so seismic noise can be measured by observing spectral bands that are devoid of normal mode peaks. For each seismogram in our data set and for each time series length employed, we estimate a spectral noise level using RMS spectral amplitude averaged over a set of such bands. For vertical component records we use four bands (1.261-1.335, 1.435-1.480, 1.895-1.940, 2.605-2.645 mHz) and for horizontal component records we use five bands (1.265-1.305, 1.445-1.470, 1.886-1.915, 3.029-3.054, 3.125-3.150 mHz). We then define SNR for each multiplet as the ratio of peak multiplet amplitudes to the estimated noise levels.

These SNR estimates are particularly useful for plotting measures of residual misfits resulting from GSF regressions. To quantify misfit in the spectral bands used to analyze each multiplet group, we employ misfit ratio (MR). This quantity is defined by

$$\mathtt{MR} = \left(\frac{\sum_{i=1}^{I} \left[(s(\omega_i) - s'(\omega_i) \right]^2}{\sum_{i=1}^{I} s^2(\omega_i)} \right), \qquad (13)$$

where $s(\omega_i)$ is the data spectrum for a given record and $s'(\omega_i)$ is the corresponding synthetic spectrum, computed with the estimated structure coefficients. Phase and amplitude contributions to the misfit are examined separately, using phase misfit and amplitude misfit. Phase misfit is the average, across the frequency band analyzed, of the difference between the phases of the data and synthetic spectra. Amplitude misfit is the average of the difference between unity and the ratio of the amplitude of the synthetic to that of the data. Figure 12 provides sample plots of these misfits against log(SNR) for the multiplet group ${}_0T_{18}$-${}_0S_{17}$-${}_2S_{11}$.

In general, we have found that smoothed curves resulting in least squares fits to such plots are closely approximated by quadratic curves which asymptotically approach a minimum at high SNR. This is illustrated by the curves shown in Figure 12. MR, phase misfits, and amplitude misfits that result from seismic noise alone are expected to decrease monotonically and asymptotically to zero. This is demonstrated by Figure 13, which results from comparing synthetic spectra of ${}_0T_{18}$-${}_0S_{17}$-${}_2S_{11}$ to otherwise equivalent spectra contaminated by artificial noise at observed noise levels. For this reason, the nonzero high SNR (HSNR) asymptotes of Figure 12 can be interpreted as expressions of the theoretical error which are uncontaminated by seismic noise.

In Table 7, the fit to the data given by the estimated structure coefficients is compared to the fits produced by predictions from aspherical mantle models. The four misfit statistics included are (1) MR averaged over all records used in each regression; (2) HSNR misfit, which is the asymptotic value of the quadratic curve fit to MR versus log(SNR); (3) HSNR amplitude misfit, defined similarly; and (4) HSNR phase misfit. For poorly excited multiplets the HSNR misfits can be difficult to estimate accurately, and care has been taken to insure that the reported misfits are robust.

Mean misfits and HSNR misfits provide significantly different information about the regressions. Mean misfits are related to the quantity minimized in each regression, and successful regressions should produce mean misfits lower than those resulting from model predictions. Mean misfits are also strong functions of the average SNR of the data set used. Consequently, mean misfits cannot meaningfully be compared between multiplets or across different data sets, since the noise contents for different multiplets or different data sets may differ. The HSNR misfits included in Table 7 are generally more useful statistics since they estimate quantities that should be largely independent of SNR. HSNR misfits are used as a tool for assessing the regressions, as described in section 4.3, and to model the effects of theoretical noise, as in section 5.1.

Table 6. Regression Inputs

Index	Specified Multipets	Specified Cross-Coupling	Highest Degrees Specified	Number of Coefficients Specified	Number of Events	Number of Horizontal Records	Number of Vertical Records	Nearby Multiplets
1	${}_0S_3$		2	7	4	0	30	
2	${}_0S_4$		8	46	16	4	182	
3	${}_0S_5$		8	46	23	9	345	
4	${}_0S_6$		8	46	25	57	495	
5	${}_0S_7,{}_2S_3$		8,6	75	18	0	287	${}_0T_7,{}_1T_1$
6	${}_0S_8$		12	92	32	57	553	${}_4S_1,{}_0T_9$
7	${}_0S_9,{}_0T_{10}$		12,6	121	32	50	500	${}_1T_4$
8	${}_0S_{10},{}_0T_{11}$	${}_0S_{10}$-${}_0T_{11}$	8,14,2	172	33	526	1036	${}_4S_2$
9	${}_0T_{12},{}_0S_{11}$, ${}_2S_7$	${}_0T_{12}$-${}_0S_{11}$ ${}_0T_{12}$-${}_2S_7$ ${}_0S_{11}$-${}_2S_7$	8,14,8, 6,6,6	275	33	512	1018	
10	${}_0T_{13},{}_0S_{12}$	${}_0T_{13}$-${}_0S_{12}$	12,16,4	260	24	434	835	${}_6S_1$
11	${}_0T_{14},{}_0S_{13}$	${}_0T_{14}$-${}_0S_{13}$	12,16,4	260	24	421	818	${}_5S_2,{}_1T_7$
12	${}_0T_{15},{}_2S_9$, ${}_2T_2,{}_0S_{14}$	${}_0T_{15}$-${}_0S_{14}$ ${}_2S_9$-${}_0S_{14}$	10,14, 8,4,7	273	33	503	992	
13	${}_0T_{16},{}_0S_{15}$	${}_0T_{16}$-${}_0S_{15}$	12,16,4	260	33	521	1063	
14	${}_0T_{17},{}_0S_{16}$	${}_0T_{17}$-${}_0S_{16}$	12,16,4	260	33	511	1027	${}_1T_9$
15	${}_0T_{18},{}_0S_{17}$, ${}_2S_{11}$	${}_0T_{18}$-${}_0S_{17}$ ${}_0S_{17}$-${}_2S_{11}$	12,16, 10,4,8	324	33	503	1001	${}_3S_6$
16	${}_0T_{19},{}_0S_{18}$	${}_0T_{19}$-${}_0S_{18}$	10,16,6	248	33	510	978	${}_3S_7$
17	${}_0T_{20},{}_0S_{19}$	${}_0T_{20}$-${}_0S_{19}$	12,16,6	273	32	375	901	
18	${}_0S_{20},{}_0T_{21}$, ${}_2S_{13}$	${}_0S_{20}$-${}_0T_{21}$	14,12 8,4	273	33	459	948	${}_8S_1,{}_2T_8$
19	${}_0S_{21}$		16	154	25	0	634	${}_1S_{14},{}_0T_{22},{}_5S_6$
20	${}_1S_2$		4	16	4	2	24	
21	${}_1S_3,{}_3S_1$	${}_1S_3$-${}_3S_1$	6,2,4	50	17	0	256	${}_0T_5$
22	${}_1S_4$		6	27	15	12	160	
23	${}_1S_5,{}_2S_4$	${}_1S_5$-${}_2S_4$	10,8,9	168	23	0	446	${}_0T_8$
24	${}_2S_5,{}_1S_6$	${}_2S_5$-${}_1S_6$	8,8,7	128	16	86	181	
25	${}_1S_7$		10	67	16	1	210	
26	${}_1S_8$		12	92	20	0	284	
27	${}_1S_9$		8	46	12	1	118	${}_0T_{13}$-${}_0S_{12}$
28	${}_1S_{10}$		8	46	15	0	125	${}_0T_{14}$-${}_0S_{13}$
29	${}_1S_{14}$		4	16	8	82	212	${}_0S_{21},{}_0T_{22},{}_5S_6$
30	${}_2S_6$		10	67	18	155	169	
31	${}_2S_8$		8	46	20	167	370	${}_4S_3$
32	${}_2S_{10},{}_4S_5$	${}_2S_{10}$-${}_4S_5$	8,8,7	118	20	143	301	
33	${}_2S_{12}$		8	46	5	55	172	${}_5S_5,{}_2T_7$
34	${}_3S_2$		4	16	10	0	90	
35	${}_3S_6$		6	29	2	68	93	${}_0T_{18}$-${}_0S_{17}$-${}_2S_{11}$
36	${}_3S_7,{}_5S_5$	${}_3S_7$-${}_5S_5$	6,8,2	80	17	7	215	${}_0T_{19}$-${}_0S_{18}$
37	${}_3S_8,{}_6S_3$	${}_3S_8$-${}_6S_3$	8,6,7	101	22	91	233	
38	${}_3S_9$		6	29	4	39	54	${}_1T_{12},{}_1S_{14},{}_0T_{21}$
39	${}_4S_1$		2	7	2	12	66	${}_0S_8$
40	${}_4S_2$		4	16	2	64	113	${}_0S_{10}$-${}_0T_{11}$
41	${}_4S_3$		6	29	20	96	357	${}_2S_8$
42	${}_4S_4,{}_1T_8$	${}_4S_4$-${}_1T_8$	6,6,7	84	16	102	163	
43	${}_5S_2$		2	7	2	0	104	${}_0T_{14}$-${}_0S_{13},{}_1T_7$
44	${}_5S_3$		6	29	17	93	166	
45	${}_5S_4,{}_2T_4$	${}_5S_4$-${}_2T_4$	6,4,7	81	22	61	394	
46	${}_5S_6$		10	67	9	0	182	${}_0S_{21}$-${}_0T_{22}$
47	${}_6S_1$		2	7	2	61	113	${}_0T_{13}$-${}_0S_{12}$
48	${}_8S_1$		2	7	5	0	132	${}_0S_{20}$-${}_0T_{21},{}_2S_{13}$
49	${}_0T_4$		2	7	3	17	0	
50	${}_0T_5$		8	46	4	66	0	${}_1S_3$-${}_3S_1$
51	${}_0T_6$		6	29	16	151	0	
52	${}_0T_7,{}_1T_1$		6,2	36	5	104	0	${}_0S_7,{}_2S_3$
53	${}_0T_8$		6	29	12	151	0	${}_1S_5$-${}_2S_4$
54	${}_0T_9$		6	29	13	205	0	${}_0S_8,{}_2S_5$-${}_1S_6$
55	${}_0T_{22}$		6	29	18	182	0	${}_1S_{14},{}_0S_{21},{}_5S_6$
56	${}_1T_2$		2	7	2	66	0	
57	${}_1T_3$		2	7	2	81	0	
58	${}_1T_4$		4	16	9	49	0	${}_0S_9$-${}_0T_{10}$
59	${}_1T_5$		6	29	14	388	0	${}_0S_{10}$-${}_0T_{11}$
60	${}_1T_6$		8	46	14	176	0	
61	${}_1T_7$		6	29	22	417	0	${}_5S_2,{}_0T_{14}$-${}_0S_{13}$
62	${}_1T_9$		6	29	18	462	0	${}_0T_{17}$-${}_0S_{16}$
63	${}_2T_8$		6	29	12	283	0	${}_0S_{20}$-${}_0T_{21},{}_2S_{13}$

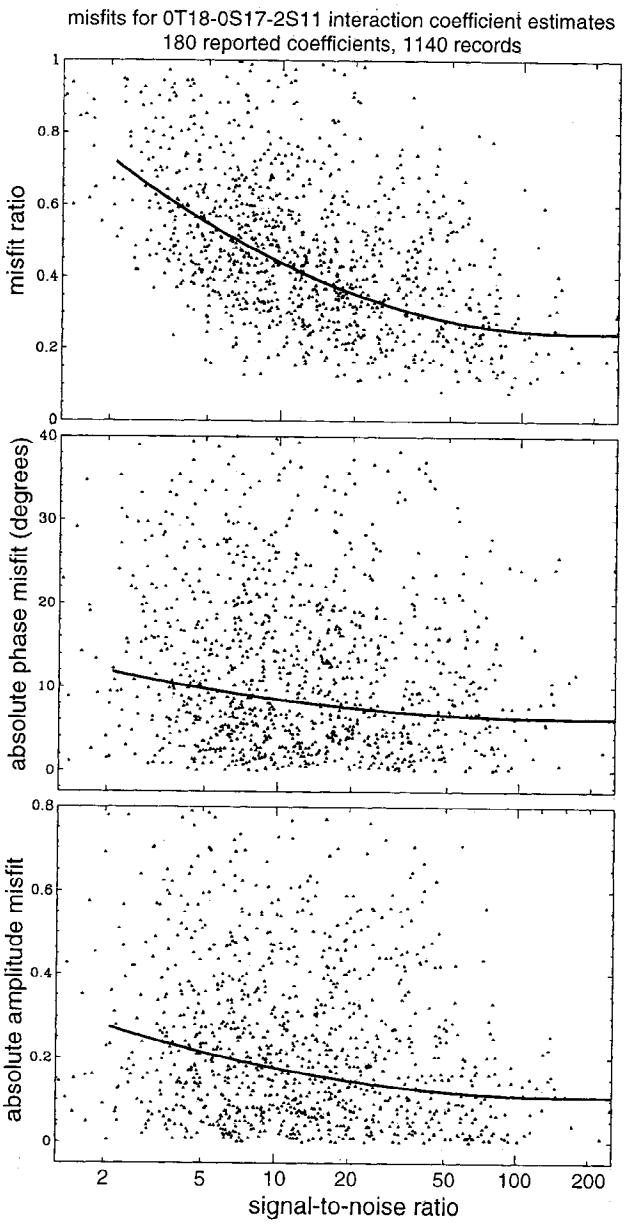

Figure 12. Variation of misfit with SNR in GSF residuals. Misfit ratio, amplitude misfit, and phase misfit are defined in section 4.2. Residuals are from a comparison of the data subset employed in preliminary analyses of ${}_0T_{18}$-${}_0S_{17}$-${}_2S_{11}$ to synthetics computed using the reported structure coefficients for these multiplets. The smooth "best fit" trends result from a least squares fit which employs a quadratic (in log(SNR)) between SNR=3 and SNR=70, and a horizontal line (asymptote) above SNR=70.

4.3. Assessing Regression Results

Because we seek to specify in the regressions as many relevant structure coefficients as possible for each multiplet group, we have established a protocol for insuring that regressions are not underspecified and for identifying estimates which are sufficiently accurate to be reported. We require that reported estimates of structure coefficients display both internal consistency, meaning that coefficients of multiplets with similar sensitivities to mantle structures should be similar, and external consistency, meaning that coefficient estimates should provide better fits to the data than do recent mantle models, while exhibiting consistency with the predictions of those models. We also confirm, whenever pos-

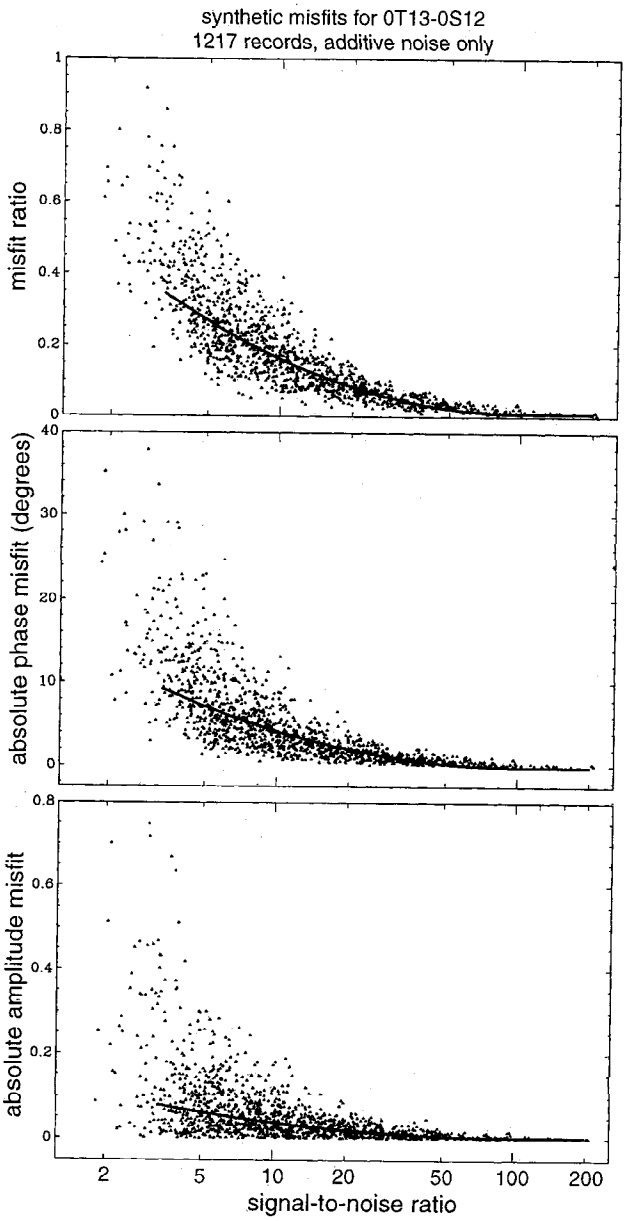

Figure 13. Simulated variation with SNR of the misfit between noise-free synthetics and synthetics contaminated by additive noise only. Noise-free synthetics are made using ${}_0T_{18}$-${}_0S_{17}$-${}_2S_{11}$ structure coefficients predicted by model S16B30. The additive noise synthetics are noise-free synthetics perturbed at each frequency by additive noise of random phase with RMS amplitude matching the observed SNR of each real data record. The best fit trends are computed as in Figure 12.

Table 7. Regression Fits

Target	Mean Misfit		HSNR Misfit		Amplitude Misfit, %		Phase Misfit, deg	
Multipets	Model[a]	GSF	Model[a]	GSF	Model[a]	GSF	Model[a]	GSF
${}_0S_3$	0.51	0.50	-	-	-	-	-	-
${}_0S_4$	0.49	0.47	0.19	0.17	11.9	11.8	3.3	2.3
${}_0S_5$	0.42	0.39	0.12	0.10	8.0	8.6	2.2	1.6
${}_0S_6$	0.42	0.40	0.11	0.09	8.0	7.2	3.1	1.8
${}_0S_{7,2}S_3$	0.46	0.38	0.30	0.16	14.1	12.6	4.7	3.4
${}_0S_8$	0.40	0.37	0.22	0.14	11.0	8.4	5.9	3.7
${}_0S_{9,0}T_{10}$	0.38	0.33	0.18	0.12	11.6	10.2	5.4	2.3
${}_0S_{10}$-${}_0T_{11}$	0.50	0.43	0.23	0.15	17.7	12.6	6.6	3.0
${}_0T_{12}$-${}_0S_{11}$-${}_2S_7$	0.54	0.46	0.28	0.20	17.5	13.7	7.9	4.8
${}_0T_{13}$-${}_0S_{12}$	0.49	0.46	0.28	0.26	19.2	19.3	7.7	6.7
${}_0T_{14}$-${}_0S_{13}$	0.53	0.44	0.28	0.17	22.0	14.8	8.8	4.1
${}_0T_{15}$-${}_0S_{14}$-${}_2S_{9,2}T_2$	0.61	0.46	0.38	0.21	30.5	18.4	12.3	5.5
${}_0T_{16,0}S_{15}$	0.56	0.47	0.34	0.21	26.8	20.5	11.7	4.7
${}_0T_{17,0}S_{16}$	0.58	0.46	0.35	0.21	28.1	20.1	11.2	4.7
${}_0T_{18,0}S_{17,2}S_{11}$	0.61	0.48	0.37	0.25	30.4	19.3	10.4	5.5
${}_0T_{19,0}S_{18}$	0.61	0.47	0.38	0.24	30.4	18.1	10.2	5.9
${}_0T_{20}$-${}_0S_{19}$	0.67	0.54	0.42	0.27	39.6	25.0	11.7	6.0
${}_0S_{20}$-${}_0T_{21}$-${}_2S_{13}$	0.63	0.48	0.38	0.26	28.7	20.3	10.4	5.1
${}_0S_{21}$	0.59	0.50	0.36	0.28	31.2	22.8	9.7	7.4
${}_1S_2$	0.49	0.47	-	-	-	-	-	-
${}_1S_3$-${}_3S_1$	0.51	0.45	0.15	0.13	7.5	4.2	2.5	2.9
${}_1S_4$	0.29	0.28	0.12	0.09	5.1	5.1	2.1	1.3
${}_1S_5$-${}_2S_4$	0.48	0.45	0.22	0.13	7.5	4.9	3.7	2.7
${}_2S_5$-${}_1S_6$	0.51	0.41	0.31	0.17	18.5	6.1	6.4	2.3
${}_1S_7$	0.53	0.35	0.23	0.08	20.4	4.7	3.6	2.3
${}_1S_8$	0.47	0.37	0.20	0.09	7.4	4.3	6.0	1.9
${}_1S_9$	0.55	0.42	0.29	0.12	13.1	5.6	5.0	3.5
${}_1S_{10}$	0.67	0.46	0.57	0.25	9.9	5.9	23.0	9.3
${}_1S_{14}$	0.71	0.68	0.36	0.31	30.8	25.6	9.7	7.9
${}_2S_6$	0.45	0.39	0.17	0.14	12.0	12.2	4.3	1.8
${}_2S_8$	0.49	0.45	0.17	0.13	11.5	10.4	3.8	2.9
${}_2S_{10,4}S_5$	0.77	0.64	0.40	0.25	17.8	18.3	16.5	7.0
${}_2S_{12}$	0.72	0.71	0.50	0.48	31.4	32.2	13.8	13.5
${}_3S_2$	0.94	0.48	-	-	-	-	-	-
${}_3S_6$	0.65	0.61	0.32	0.29	17.3	17.0	6.6	5.3
${}_3S_7$-${}_5S_5$	0.55	0.42	0.31	0.21	18.2	12.0	6.5	4.8
${}_3S_9$	0.56	0.53	-	-	-	-	-	-
${}_3S_8$-${}_6S_3$	0.86	0.43	0.73	0.10	48.5	9.7	32.4	2.9
${}_4S_1$	0.38	0.38	0.19	0.17	19.2	14.7	5.1	5.4
${}_4S_2$	0.50	0.50	0.26	0.27	20.7	19.5	7.4	6.4
${}_4S_3$	0.63	0.59	0.28	0.14	12.0	7.6	7.2	3.0
${}_4S_4$-${}_1T_8$	0.59	0.53	0.37	0.25	19.4	12.8	9.6	5.3
${}_5S_2$	0.52	0.50	0.13	0.13	8.3	4.9	2.9	2.9
${}_5S_3$	0.72	0.56	0.33	0.09	13.9	4.6	6.0	1.6
${}_5S_4$-${}_2T_4$	0.61	0.46	0.38	0.14	22.5	7.6	11.6	3.0
${}_5S_6$	0.50	0.36	0.24	0.11	11.1	10.4	4.8	2.9
${}_6S_1$	0.70	0.60	0.41	0.27	23.1	16.0	10.8	5.4
${}_8S_1$	0.69	0.58	0.58	0.33	31.6	21.2	18.4	8.9
${}_0T_4$	0.45	0.40	-	-	-	-	-	-
${}_0T_5$	0.44	0.39	-	-	-	-	-	-
${}_0T_6$	0.61	0.58	0.29	0.25	10.5	9.5	6.3	1.5
${}_0T_{7,1}T_1$	0.52	0.48	0.12	0.09	6.0	4.3	0.8	1.8
${}_0T_8$	0.51	0.49	0.20	0.17	5.9	8.3	7.0	6.8
${}_0T_9$	0.43	0.45	0.16	0.16	11.4	12.5	2.4	5.9
${}_0T_{22}$	0.63	0.58	0.32	0.31	31.1	32.6	3.5	7.0
${}_1T_2$	0.69	0.69	-	-	-	-	-	-
${}_1T_3$	0.56	0.52	-	-	-	-	-	-
${}_1T_4$	0.37	0.34	-	-	-	-	-	-
${}_1T_5$	0.57	0.57	0.11	0.12	9.8	10.2	1.8	2.0
${}_1T_6$	0.60	0.56	0.17	0.13	8.7	2.1	6.2	4.3
${}_1T_7$	0.49	0.49	0.20	0.19	12.7	13.9	1.8	2.3
${}_1T_9$	0.46	0.45	0.21	0.20	16.6	16.6	4.5	3.6
${}_2T_8$	0.66	0.64	0.43	0.33	55.6	51.3	13.9	14.8

[a]Listed misfits are the lesser of the misfits produced by models S12_WM13 and SH.10c.17.

sible, that the specification of structure coefficients for cross-coupling or structures of degrees $s > 4$ improves the consistency of other coefficients. In assessing fits to the data, we employ the average and HSNR misfits of Table 7. To address other issues of consistency we use the lateral correlation and relative amplitudes of splitting functions.

4.3.1. Internal consistency. A useful check of the internal consistency of the estimated structure coefficients is the lateral correlation of splitting functions along the same overtone branch, because modal sensitivity to Earth structure tends to vary smoothly along each branch (with certain known exceptions). The thick solid lines in Figure 14 plot the confidence of the geographical correlation between the estimated coefficients for multiplets of adjacent l values along several modal branches. Correlation confidence, as defined by *Eckhardt* [1984], is useful for comparing correlations at different harmonic degrees. Estimated structure coefficients along the overtone branches are usually correlated with better than 90% confidence. Exceptions are greatest when strong coupling occurs between pairs (e.g., ${}_1S_5$-${}_2S_4$, ${}_1S_6$-${}_2S_5$) or trios of multiplets (e.g., ${}_0T_{12}$-${}_0S_{11}$-${}_2S_7$, ${}_0T_{15}$-${}_0S_{14}$-${}_2S_9$, and ${}_0T_{18}$-${}_0S_{17}$-${}_2S_{11}$). Reported coefficients exhibiting relatively weak along-branch correlations, like those of degree 4 for multiplet ${}_0T_{10}$ and degree 8 of ${}_0S_{11}$, are generally assigned larger uncertainties.

Further confidence in the results is established by geographic consistency between estimated splitting functions of multiplets from different branches with similar sensitivity kernels. The strong similarities of the degree 2-8 splitting functions of ${}_0S_{17}$, ${}_0T_{18}$, and ${}_2S_{11}$, shown in Plate 1, are an example of such consistency.

4.3.2. External consistency. As in the example of Figure 3, synthetic spectra generated using GSF structure coefficient estimates usually fit data better than do synthetics constructed using recent mantle models. Table 7 documents misfit for each multiplet group analyzed. In addition to providing misfit statistics for the estimated coefficients, average and HSNR misfits are listed for either S12_WM13 or SH.10c.17, depending upon which model fits the data better for the specified mode group. In nearly every case, the estimated structure coefficients provide better fits to the normal mode multiplets than the predictions of either model, both in an averaged sense and for HSNR data. The coefficient estimates usually fit both phase and amplitude data better than the models. Preliminary investigations suggest that the newer mantle models MK12_WM13, S16B30, and SAW12D probably fit the these spectra no better than the older models S12_WM13 and SH.10c.17.

The thin lines of Figure 14 show the confidence of correlation between structure coefficients predicted by models S12_WM13 and SH.10c.17. The dashed lines plot correlations between the estimated coefficients and whichever of these two models best agrees with the estimates. The most important characteristic of these plots

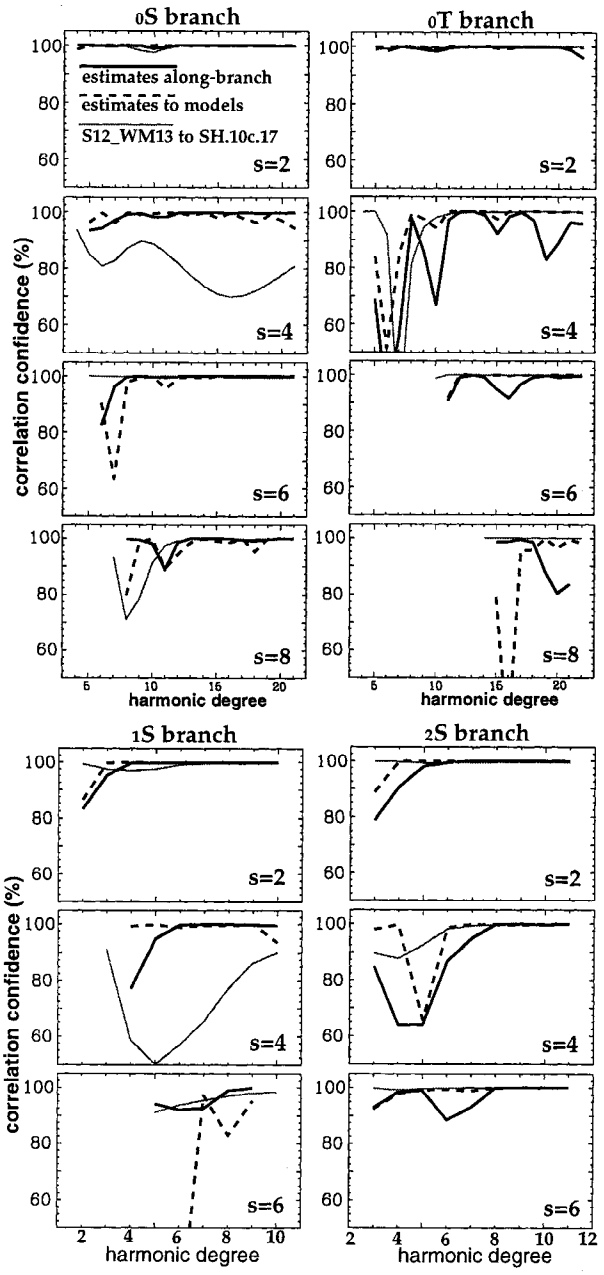

Figure 14. Correlation confidence levels for internal and external consistency checks of the GSF coefficient estimates. The along-branch trends (thick solid lines) compare estimated structure coefficients of adjacent multiplets on the same overtone branch. Also shown are the correlations of the estimates to either SH.10c.17 or S12_WM13, whichever agrees better with the measurements (dashed lines). Correlations between these two models (thin solid lines) are displayed for comparison.

is that the GSF estimates usually correlate with at least one model better than the models correlate with each other. Thus, while the new normal modal coefficients differ substantially from model predictions, they are not inconsistent with existing constraints on the Earth's interior structure.

Figure 15 displays the primary difference between model predictions and the GSF structure coefficients. These plots show the root-mean-square (RMS) amplitude of the coefficients as a function of structural degree for both the models and our estimates. While both predicted and measured structure coefficients are largest at degree 2, the estimates are consistently larger than predicted coefficients at degrees 4, 6, and 8 of structure, especially for the ${}_0T$ and ${}_2S$ modes which are dominantly sensitive to the upper mantle and transition zone. This may imply a somewhat flatter, or whiter, spectrum of heterogeneity within these regions of the Earth than anticipated by the models. Such implications are discussed further in section 6.

4.3.3. New coefficients and improved consistency. The new normal mode catalogue includes cross-coupling structure coefficients and many new estimates of coefficients at $s > 4$. These coefficients exhibit internal and external consistency similar to those of self-coupling coefficients at degrees 2 and 4. To establish confidence in $s > 4$ and cross-coupling coefficient estimates still more firmly we note two additional characteristics. First, we observe that regressions specifying these coefficients generally improve the external and internal consistency of other estimates. Examples of such observations for cross-coupling are documented in Tables 3 and 4 and by *Resovsky and Ritzwoller* [1995a]. Examples for $s > 4$ are presented by *Ritzwoller and Resovsky* [1995]. Second, we observe that specification of $s > 4$ and cross-coupling coefficients usually improves not only average misfit but also HSNR misfit, amplitude misfit, and phase misfit. Table 8 gives examples of improvements achieved by extending our analyses to the highest specified degree ($s_{\max}$, column 4 of Table 6) and the specification of structural coupling. Almost all of the HSNR misfits listed are reduced by more than 20% when more detailed structures are specified.

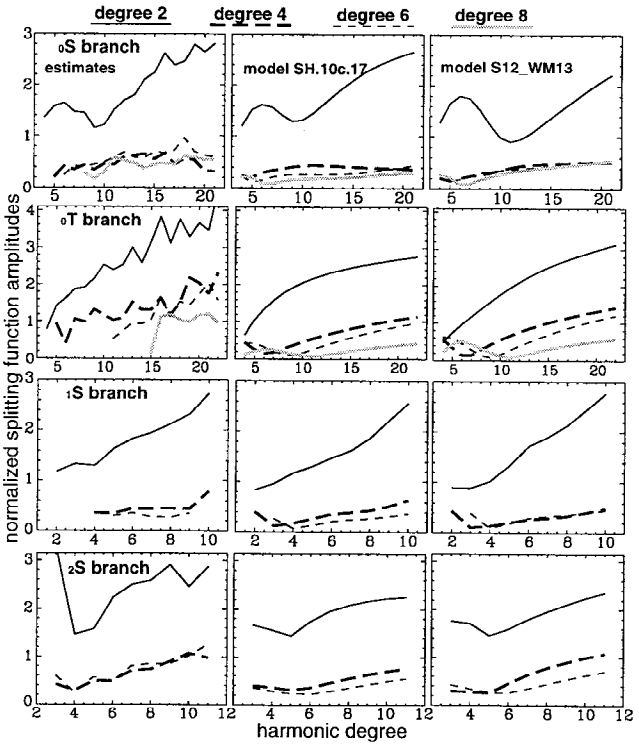

Figure 15. RMS amplitude of the observed structure coefficients at each degree of structure. The amplitudes are normalized by the degenerate frequencies of the multiplets. Amplitudes predicted by models SH.10c.17 and S12_WM13 are also shown.

5. Assigning Uncertainty

Standard error analyses underestimate uncertainties in structure coefficients obtained from GSF. This failure is attributable to theoretical errors (section 3.1) and to covariances among the structure coefficients (section 3.2), which are not usually incorporated in normal mode error analyses. The error analysis technique we employ uses regressions performed on synthetic data with simulated theoretical errors to assess the combined effects of these errors and covariances.

5.1. Simulating Error

Rather than identifying and synthesizing each component of the theoretical error, we have found it more efficient to assess the net cumulative impact of these

Table 8a. Improving HSNR Misfits by Specifying Higher Degrees

	Degrees 0-4 Specified			Degrees 0-$s_{\max}$ Specified		
Multiplets	MR[a]	AM,[b] %	PM,[c] deg	MR	AM, %	PM, deg
${}_0S_8$	.20	5.0	4.1	.13	4.5	3.5
${}_1S_8$	.19	1.5	5.1	.06	0.7	2.8
${}_2S_6$	.18	11.8	3.7	.12	7.9	2.0
${}_0S_{20}$-${}_0T_{21}$-${}_2S_{13}$	.37	15.5	8.8	.31	13.7	6.6

[a]HSNR misfit ratio.
[b]HSNR amplitude misfit.
[c]HSNR phase misfit.

Table 8b. Improving HSNR Misfits by Specifying Coupling

	Structural Coupling Unspecified			Structural Coupling Specified		
multiplets	MR	AM, %	PM, deg	MR ratio	AM, %	PM, deg
${}_2S_5$-${}_1S_6$	.29	15.0	7.6	.10	2.5	2.5
${}_5S_4$-${}_2T_4$	.32	8.8	8.8	.13	4.7	3.1
${}_0T_{20}$-${}_0S_{19}$	.39	15.8	9.5	.31	13.8	7.9
${}_3S_8$-${}_6S_3$	.26	10.1	9.9	.10	6.1	5.6

errors by simulating observed characteristics of misfits to HSNR data obtained with the estimated coefficients. For each seismogram j and each multiplet group k the simulated data may be represented by

$$ {}_k s_j^{\text{data}}(\omega) \approx {}_k s_j^{\text{simul}}(\omega) = n_j(\omega) + {}_k T_j(\omega) {}_k s_j^{\text{synth}}(\omega). \quad (14) $$

${}_k s_j^{\text{synth}}(\omega)$ is a complex synthetic spectrum produced using the estimated structure coefficients, $n_j(\omega)$ is additive noise, and ${}_k T_j(\omega)$ is a complex transfer function with which we model theoretical errors.

Synthetic additive noise at each discrete frequency of each spectrum is created using a random deviate which imitates the statistical properties of observed seismic noise and has the average amplitude measured for the corresponding data spectrum, described in section 4.2. This form of additive noise was used to produce Figure 13.

We approximate ${}_k T_j(\omega)$ using two important assumptions. The first is that for each seismogram the transfer function for each multiplet group analyzed is a low-order polynomial function of frequency. The amplitude transfer function is the ratio of data amplitude to synthetic amplitude. The phase transfer function is the difference between the (unwrapped) phases of data and synthetic spectra. As Figure 16 demonstrates, most of the misfit in the data can be accounted for by linear transfer functions in amplitude and phase. We have found it adequate to use linear functions in simulating the data.

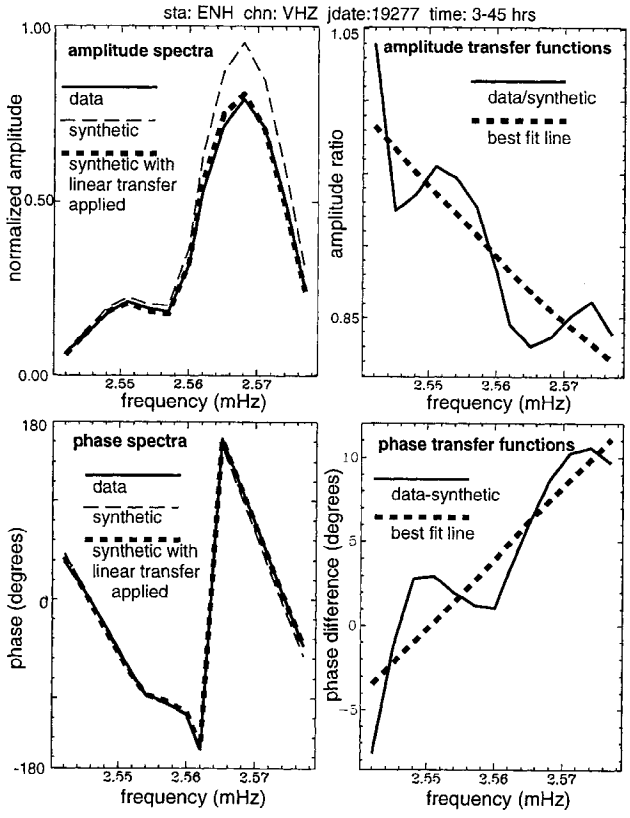

Figure 16. Sample transfer functions in amplitude and phase and linear fits to these functions. (left) Amplitude and phase spectra of ${}_0T_{18}$-${}_0S_{17}$-${}_2S_{11}$. The solid lines are data spectra, the thin dashed lines are noise-free synthetic spectra constructed using GSF structure coefficient estimates, and the thick dashed lines are the product of the synthetic spectra and the best fit linear approximation to the transfer functions. (right) The linear transfer functions, together with the actual transfer functions between data and synthetics.

The second assumption is that the means and slopes of the linear transfer functions that best fit the data have simple Gaussian distributions in the set of records used, independent of source-receiver geometries. This assumption allows us to use distributions observed for high SNR data to simulate theoretical errors in the whole data set, so that we need not attempt to measure theoretical error transfer functions which are obscured by noise. The thick solid histograms in Figure 17 show the distributions of the means and slopes of the linear fits to amplitude ratio and phase difference transfer functions for recordings of ${}_0T_{18}$-${}_0S_{17}$-${}_2S_{11}$ with SNR > 50. Gaussians which fit these histograms are shown as thin solid lines. Synthetic distributions of means and slopes are produced using random distributions which reproduce the observed Gaussians. The resulting transfer functions are combined with synthetic additive noise to yield our simulated data. Distributions of measured means and slopes from one such simulation of ${}_0T_{18}$-${}_0S_{17}$-${}_2S_{11}$ data are shown as dashed line histograms in Figure 17.

The assumption that the means and slopes of transfer functions are governed by Gaussian distributions is more questionable than the assumption that theoretical errors are manifest as linear transfer functions. However, comparisons of observed and simulated data indicate that it is not obviously flawed. Figure 18 uses comparisons of synthetic spectra with and without simulated noise and theoretical errors to demonstrate the success of the method in duplicating the gross characteristics of observed misfit. The effects of noise and theoretical errors in Figure 18 each resemble those displayed by the observed misfits of Figure 12.

5.2. Monte Carlo Approximation of Uncertainty

After a set of structure coefficients have been estimated with GSF for a given multiplet group, these coefficients are used to construct synthetic spectra for each seismogram in the data. Following equation (14), these spectra are modified with synthetic additive noise and the transfer functions which simulate theoretical error. GSF is then applied to these noisy synthetics, and the resulting coefficient estimates are compared with the original estimates. Because these regressions imitate the original GSF analyses, the effect of covariances is incorporated in simulating the effect of error on structure coefficient estimates.

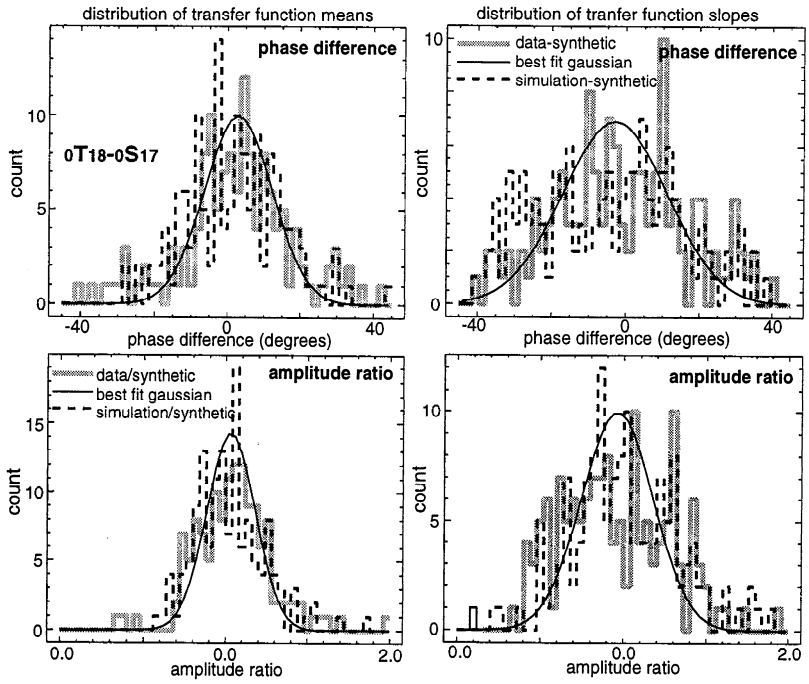

Figure 17. Sample distributions of (left) means and (right) slopes for best fit linear transfer functions in (top) phase difference and (bottom) amplitude ratio, for recordings of ${}_0T_{18}$-${}_0S_{17}$-${}_2S_{11}$ with SNR > 50. Thick solid histograms are distributions for transfer functions between data and noise-free synthetics made using structure coefficient estimates, as in Figure 16. Gaussians fit to these distributions are shown as thin solid lines. Dashed histograms are distributions for transfer functions between noise-free synthetics and synthetics which incorporate additive noise and simulated transfer functions.

This procedure is repeated for several realizations of simulated noise and theoretical error, and the suites of coefficient reestimates are interpreted as if they resulted from "Monte Carlo" sampling of real data. That is, the standard deviation of the suite of re-estimates for each coefficient, σ_s^t, is used to assign an uncertainty, usually of magnitude $2\sigma_s^t$, to the original estimates. Figure 19 demonstrates the result of this procedure for some of the coefficients of the ${}_0T_{18}$-${}_0S_{17}$-${}_2S_{11}$ group. For each coefficient, 2σ error bars centered on the original GSF estimates are superimposed on thin horizontal lines which mark the estimates resulting from each realization of the synthetic data. The assigned error bars are generally consistent with the size and distribution of differences between estimates and model predictions and with those between estimates for multiplets which sample the Earth similarly (i.e., ${}_0T_{18}$ and ${}_2S_{11}$).

5.3. Identifying Outliers

The uncertainty estimation described above uses a statistical approach to model theoretical errors using the characteristics of HSNR transfer functions. This approach assumes that the distribution of errors is identical for all sources and receivers at all times. Uncertainties estimated with this assumption can be too small when there are strong systematic errors affecting only subsets of the data. At present, we account for such cases only when they result in obvious "outliers" in our catalogue of measurements.

We use the assumption of along-branch smoothness to identify outliers. Outliers are defined as structure coefficients which are far, relative to their uncertainties, from the trend established by estimates of corresponding coefficients of similar multiplets. With "far" defined as $4\sigma_s^t$ from a smooth trend, fewer than 5% of our initial estimates are identifiable as outliers. Most of these cases appear to be attributable to unspecified structure in analyses of strongly coupling multiplet groups. The coefficients in question are "corrected" to achieve reasonable internal consistency by increasing the associated uncertainties and, where appropriate, by shifting the estimates into better alignment with along-branch trends.

Simulated bias, which is the difference between original GSF estimates and the average of the Monte Carlo reestimates, is generally smaller than the estimated uncertainty for each coefficient. Because simulated bias is expected to approximate the bias in our original estimates caused by noise and error, when significant simulated bias is observed we shift our estimates accordingly and increase coefficient uncertainties by 25% of the simulated bias. It should be noted that we do not observe

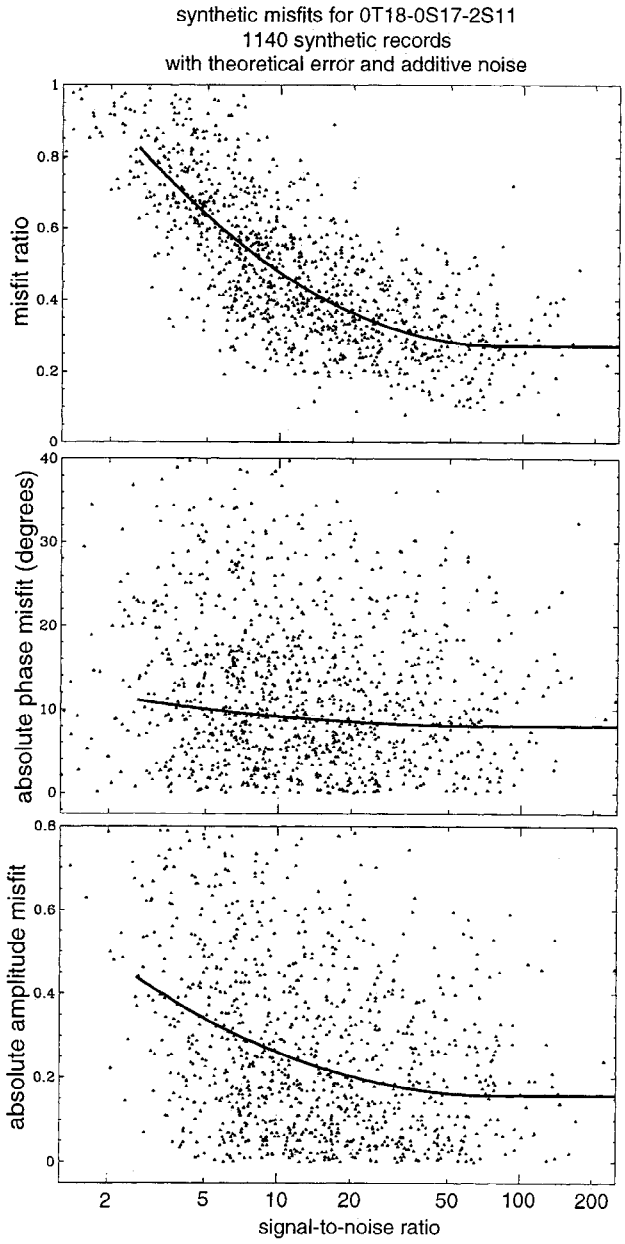

Figure 18. Simulated variation of misfit with SNR, constructed similarly to Figure 13, except that the "noisy" data include simulated theoretical error transfer functions as well as additive noise. These synthesized misfit trends compare favorably with those observed for real data, as in Figure 12.

strong bias in GSF estimates of multiplet Q, which has been reported in some other normal mode studies (J. Durek and G. Ekström, unpublished data, 1997).

6. Conclusions

To provide improved normal mode constraints on 3-D Earth structure, we have developed generalized spectral fitting and a method of performing Monte Carlo simulations to obtain reasonable estimates of uncertainty. GSF and the Monte Carlo simulations have been used to estimate more than 3100 structure coefficients and the associated uncertainties for the seismic spectrum below 3 mHz. These coefficients may be retrieved from the electronic supplement to this paper. Previously, fewer than a thousand such coefficients had been estimated for this portion of the spectrum [*Ritzwoller et al.*, 1988; *Smith and Masters*, 1989a,b; *Tromp and Zanzerkia*, 1995; *He and Tromp*, 1996].

Because these GSF regressions have reduced theoretical errors and covariances and because our error analyses account for the effects of the errors and covariances that remain, the new coefficients are generally more accurate and more precise than those of previous catalogues. The improved size, accuracy, and precision of the new catalogue imply (1) improved resolution of 3-D Earth structures, particularly in the transition zone and lower mantle, and (2) enhanced capability for assessing and comparing 3-D Earth models.

Resolution of structures in the transition zone and outermost lower mantle should be significantly improved by almost 2000 new structure coefficient estimates for the ${}_0S$, ${}_0T$, and ${}_2S$ branches. GSF has proved essential to obtaining constraints from these modes, because most are subject to strong cross-coupling through the Coriolis force and aspherical structures. Likewise, resolution of lower mantle structures has been enhanced with more than 1000 coefficient estimates from various overtone multiplets, including lower mantle shear modes of the ${}_1S$, ${}_1T$, and ${}_3S$ branches and lower mantle compressional modes of the ${}_4S$ and ${}_5S$ branches. Almost half of these multiplets either cross-couple strongly or underlie strongly cross-coupled fundamentals. GSF and the expanded long-period data set allow us to obtain constraints through degrees 6 and 8 for many of these overtones. The estimated coefficients of cross-coupling include 127 odd-degree coefficients, the first normal mode constraints on odd-degree structures, most of which are sensitive to the transition zone and lower mantle.

The improved capability for the assessment of 3-D models is illustrated by Figure 20, which displays several along-branch sets of structure coefficient estimates and predictions. The estimates from this study are plotted as thick error bars and those of earlier studies are plotted as thin error bars. Solid lines show the predictions of model SH.10c.17 and dashed lines show those of model S12_WM13. It is clear that the new suites of degrees 2 and 4 structure coefficient estimates are less uncertain and more complete and show smoother trends than those of previous studies. These coefficients are better able to discriminate between disparate model predictions. For example, it is apparent that model SH.10c.17 is favored by GSF estimates of c_2^0 and $\mathrm{Im}(c_2^2)$ for ${}_0S$ modes which are dominantly sensitive to the transition zone and upper mantle ($l \geq 10$). The new estimates often agree with SH.10c.17 predictions better than do the earlier estimates [*Ritzwoller et al.*,

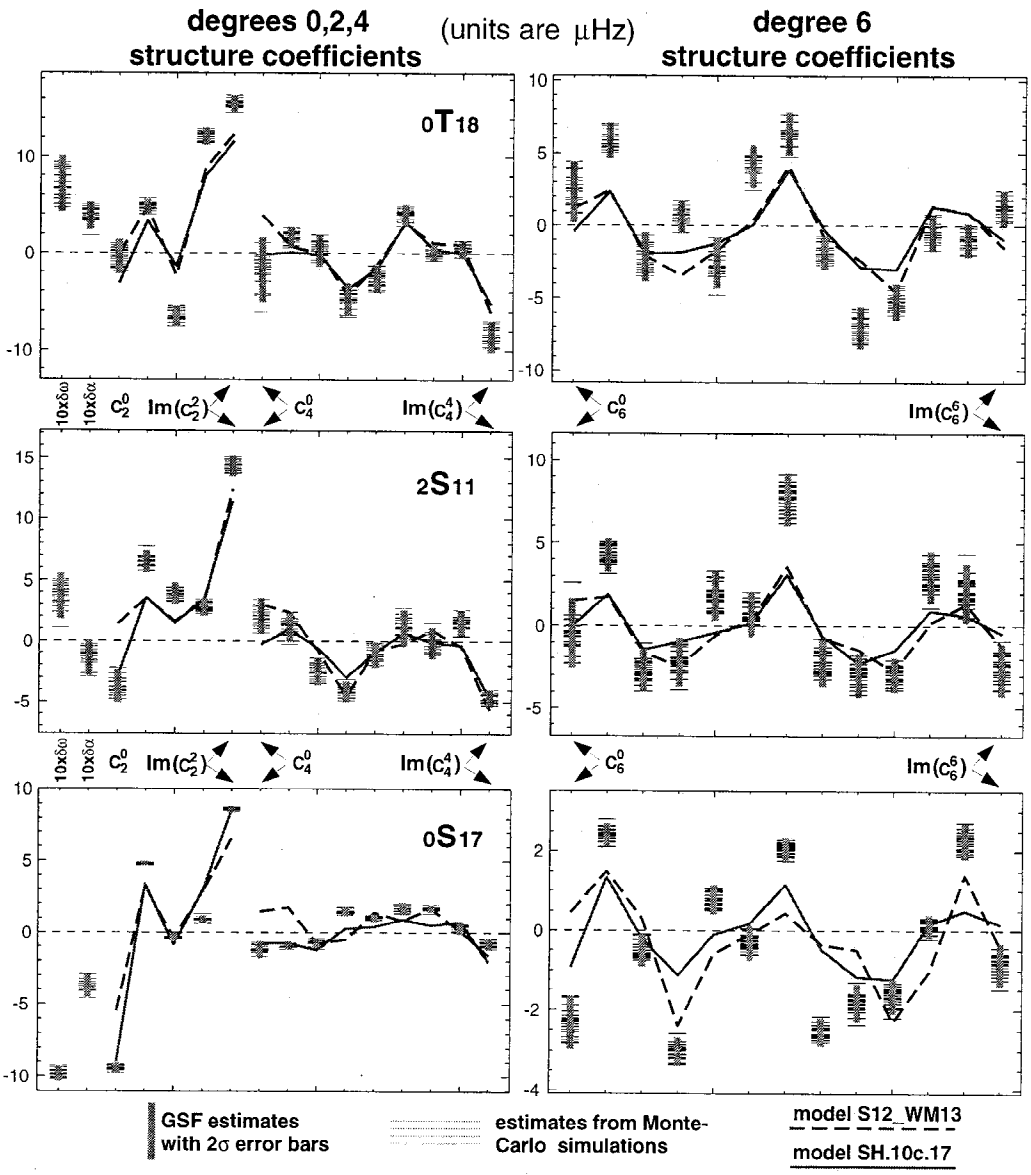

Figure 19. Results from Monte Carlo error analysis. Structure coefficient estimates as plotted as vertical error bars. The plotted coefficients are ordered as in Figure 6. Horizontal lines mark the estimates from 20 realizations of the Monte Carlo error analysis. The thick vertical error bars are centered on the averages of these distributions and have half lengths equal to 2σ for each distribution. The predictions of models S12_WM13 (dashed lines) and SH.10c.17 (solid lines) are shown for comparison. Before such estimates are catalogued, they are revised using observations of biasing and along-branch consistency.

1988; *Smith and Masters,* 1989a,b] included in the construction of that model. Conversely, c_2^0 estimates for the lower mantle ($l \leq 10$) ${}_0S$ modes, Re(c_2^2) estimates for toroidal ${}_0T$ modes and c_4^0 estimates for ${}_2S$ modes favor model S12_WM13.

GSF structure coefficient estimates at higher degrees, such as those for degrees 6 and 8 in Figure 20, also appear to be precise enough for useful model assessment. Of particular note is the difference between the amplitude of estimated splitting functions for ${}_0S$, ${}_0T$, ${}_2S$ modes and model predictions. Such modes are primarily sensitive to shear velocity in the transition zone and, as noted in section 4.3.2 and apparent in Plate 1, estimated coefficient amplitudes at degrees 6 and 8 are elevated relative the predictions of models SH.10c.17 and S12_WM13. Because of the attention given to reducing and simulating the effects of theoretical error and covariance, it is likely that this phenomenon is not an artifact of the regression technique. The spectrum of transition zone heterogeneity may well be "whiter" than that predicted by SH.10c.17, S12_WM13, and several similar models.

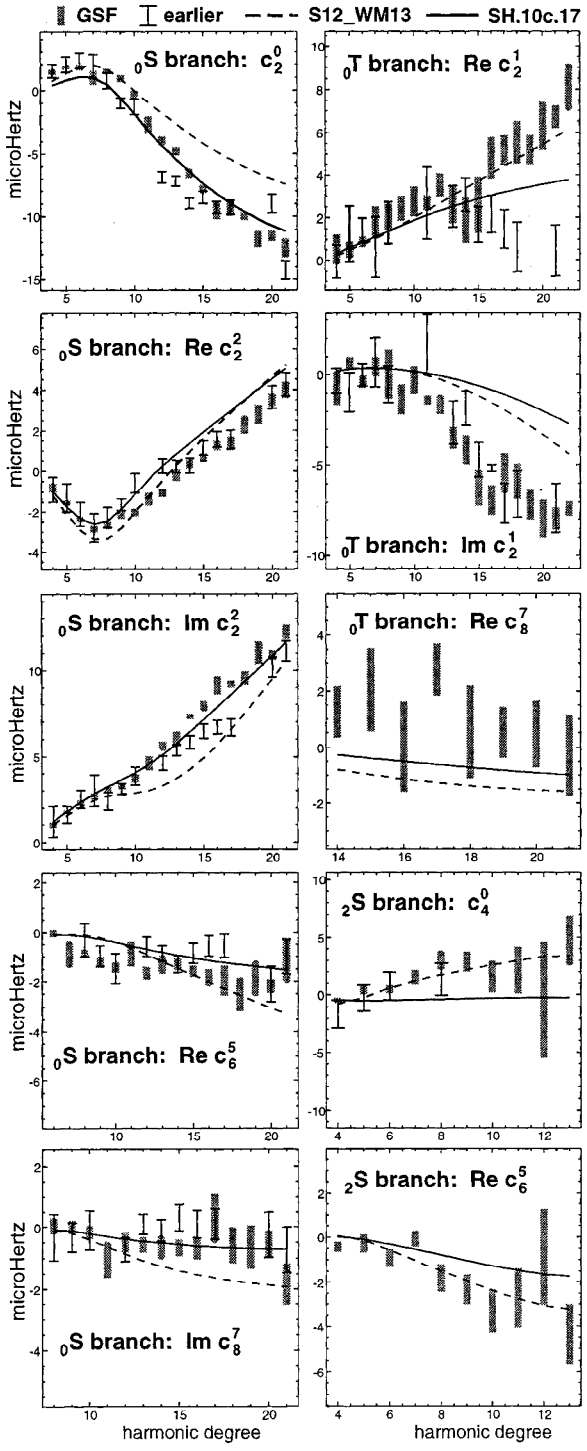

Figure 20. Sample comparisons of GSF structure coefficient estimates (thick bars), earlier structure coefficient estimates (thin bars), and the predictions of models S12_WM13 (dashed lines) and SH.10c.17 (solid lines). Earlier estimates are from the studies by *Ritzwoller et al.* [1988], *Smith and Masters* [1989a,b], and *Tromp and Zanzerkia* [1995].

We have begun to apply this and other information in the new normal mode catalogue to the refinement of 3-D Earth models [e.g., *Resovsky and Ritzwoller,* 1997]. However, it is important that the resolution of the catalogue be improved by performing normal mode analyses of similar detail to frequencies beyond 3 mHz. Given existing data and computational resources, GSF is readily adapted to the analysis of the spectrum between 3 and 5 mHz, where coupling between adjacent fundamental mode multiplets is important. Strong constraints on odd degree structure in the upper mantle should result from such analyses.

Acknowledgments. We are grateful to J. Park and J. Tromp for insightful reviews and to the following individuals for providing the high-quality digital seismic data employed extensively in this research: Duncan Agnew at UCSD (IDA data); Peter Davis at UCSD (IRIS/IDA data); Genevieve Roult at IPG (GEOSCOPE data); Bob Woodward at the ASL (IRIS/GSN data); and Tim Ahern and colleagues at the IRIS DMC at the University of Washington (GSN data). Data management software was provided by Danny Harvey and Dan Quinlan. The funding for this research was provided by NSF grants EAR-95-09836 and EAR-97-06188.

References

Anderson, H. J., and J. Zhang, Long-period seismic radiation from the May 23, 1989, Macquarie Ridge earthquake: Evidence for coseismic slip in the mantle?, *J. Geophys. Res., 96,* 19,853-19,863, 1991.

Dziewonski, A. M., and D. L. Anderson, Preliminary reference Earth model, *Phys. Earth Planet. Inter., 25,* 297-356, 1981.

Dziewonski, A. M., and W.-J. Su, 3-D models of shear and bulk velocities in the mantle *Eos Trans. AGU, 76 (17),* Spring Meet. Suppl., 41, 1995.

Eckhardt, D. H., Correlations between global features of terrestrial fields, *Math. Geol., 16,* 155-171, 1984.

Edmonds, A. R., *Angular Momentum and Quantum Mechanics,* Princeton Univ. Press, Princeton, N. J., 1960.

Ekström, G., and B. Romanowicz, The 23 May 1989 Macquarie Ridge earthquake; a very broad band analysis, *Geophys. Res. Lett., 17,* 993-999, 1990.

Forte, A. M., R.L. Woodward, and A. M. Dziewonski, Joint inversions of seismic and geodynamic data for models of three-dimensional mantle heterogeneity, *J. Geophys. Res., 99,* 21,857-21,877, 1994.

Giardini, D., X.-D. Li, and J. H. Woodhouse, Three dimensional structure of the Earth from splitting in free oscillation spectra, *Nature, 325,* 405-411, 1987.

Giardini, D., X.-D. Li, and J. H. Woodhouse, The splitting functions of long-period normal modes of the Earth, *J. Geophys. Res., 93,* 13,716-13,742, 1988.

He, X., and J. Tromp, Normal-mode constraints on the structure of the Earth, *J. Geophys. Res., 101,* 20,053-20,082, 1996.

Lawson, C., and R. Hanson, *Solving Least Squares Problems,* Prentice-Hall, Englewood Cliffs, N. J., 1974.

Li, X.-D., and B. Romanowicz, Global mantle shear-velocity model developed using nonlinear asymptotic coupling theory, *J. Geophys. Res., 101,* 22,245-22,272, 1996.

Li, X.-D., D. Giardini, and J. H. Woodhouse, Large-scale three-dimensional even-degree structure of the Earth from splitting of long-period normal modes, *J. Geophys. Res., 96,* 551-557, 1991.

Lognonné, P., Normal modes and seismograms in an anelastic rotating Earth, *J. Geophys. Res., 96,* 20,309-20,319, 1991.

Masters, G., Seismic modeling of the Earth's large-scale

three-dimensional structure, *Philos. Trans. R. Soc. London, Ser. A, 328,* 329-349, 1989.

Masters, G., J. Park and F. Gilbert, Observations of coupled spheroidal and toroidal modes, *J. Geophys. Res., 88,* 10,285-10,298, 1983.

Masters, G., H. Bolton, and P. Shearer, Large-scale 3-dimensional structure of the mantle, *Eos Trans. AGU, 73 (43),* Fall Meet. Suppl., 201, 1992.

Masters, G., S. Johnson, G. Laske, and H. Bolton, A shear-velocity model of the mantle, *Philos. Trans. R. Soc. London, Ser. A, 354,* 1385-1411, 1996.

Park, J., Synthetic seismograms from coupled free oscillations: Effects of lateral structure and rotation, *J. Geophys. Res., 91,* 6441-6464, 1986.

Park, J., and F. Gilbert, Coupled free oscillations of an aspherical, dissipative, rotating Earth: Galerkin theory, *J. Geophys. Res., 91,* 7241-7260, 1986.

Resovsky, J. S., and M. H. Ritzwoller, Effect of elastic and anelastic upper mantle models on long-period Rayleigh waves, *Eos Trans. AGU, 73 (14),* Spring Meet. Suppl., 195, 1992.

Resovsky, J. S., and M. H. Ritzwoller, Characterizing the long-period seismic effects of long-wavelength elastic and anelastic models, *Geophys. J. Int., 117,* 365-393, 1994.

Resovsky, J. S., and M. H. Ritzwoller, Constraining odd-degree mantle structure with normal modes, *Geophys. Res. Lett., 22,* 2301-2304, 1995a.

Resovsky, J. S., and M. H. Ritzwoller, Structural constraints and implications from an expanded set of mantle-sensitive normal modes, *Eos Trans. AGU, 76 (46),* Fall Meet. Suppl., 423, 1995b.

Resovsky, J. S., and M. H. Ritzwoller, Constraining 3-D Earth models using a new normal mode catalogue, paper presented at Int. Assn. of Seismol. and Phys. of Earth's Inter., 29th General Assembly, Thessaloniki, Greece, 1997.

Ritzwoller, M. H., and E. M. Lavely, Three-dimensional seismic models of the Earth's mantle, *Rev. Geophys., 33,* 1-66, 1995.

Ritzwoller, M. H., and J. S. Resovsky, The feasibility of normal mode constraints on higher degree structures, *Geophys. Res. Lett., 22,* 2305-2308, 1995.

Ritzwoller, M. H., and J. Wahr, Geodynamically consistent seismic inversion for mantle structure and internal boundary topography, *Eos Trans. AGU, 75 (44),* Fall Meet. Suppl., 663, 1994.

Ritzwoller, M. H., and J. Wahr, Normal mode constraints on mantle structure and dynamics, paper presented at Int. Union of Geod. and Geophys., XXI General Assembly, Boulder, Colorado, 1995.

Ritzwoller, M. H., G. Masters, and F. Gilbert, Observations of anomalous splitting and their interpretation in terms of aspherical structure, *J. Geophys. Res., 91,* 10,203-10,228, 1986.

Ritzwoller, M. H., G. Masters, and F. Gilbert, Constraining aspherical structure with low harmonic degree interaction coefficients: Application to uncoupled multiplets, *J. Geophys. Res., 93,* 6269-6396, 1988.

Silver, P. G., and T. H. Jordan, Fundamental spheroidal mode observations of aspherical heterogeneity, *Geophys. J. R. Astron. Soc., 64,* 605-634, 1981.

Smith, M. F., and G. Masters, Aspherical structure constraints from normal mode frequency and attenuation measurements, *J. Geophys. Res., 94,* 1953-1976, 1989a.

Smith, M. F., and G. Masters, The effect of Coriolis coupling of free oscillation multiplets on the determination of aspherical Earth structure, *Geophys. Res. Lett., 16,* 263-266, 1989b.

Su, W.-J., and A. M. Dziewonski, Predominance of long-wavelength heterogeneity in the mantle, *Nature, 352,* 121-126, 1991.

Su, W.-J., and A. M. Dziewonski, Degree 12 model of shear velocity heterogeneity in the mantle, *J. Geophys. Res., 99,* 6945-6980, 1994.

Tromp, J., Support for anisotropy of the Earth's inner core, *Nature, 366,* 678-681, 1993.

Tromp, J., Normal mode splitting due to inner core anisotropy, *Geophys. J. Int., 121,* 963-968, 1995.

Tromp, J., and E. Zanzerkia, Toroidal splitting observations from the great 1994 Bolivia and Kuril Islands earthquakes, *Geophys. Res. Lett., 22,* 2297-3000, 1995.

Um, J., G. Masters, and F. Gilbert, Splitting of Earth's normal modes observed from the Bolivian earthquake, *Eos Trans. AGU, 75 (44),* Fall Meet. Suppl., 468, 1994.

Velasco, A., C. Ammon, and T. Lay, Source time function complexity of the great 1989 Macquarie Ridge earthquake *J. Geophys. Res., 100,* 3989-4009, 1995.

Widmer, R., W. Zurn, and G. Masters, Observations of low-order toroidal modes from the 1989 Macquarie Rise event, *Geophys. J. Int., 104,* 226-236, 1992a.

Widmer, R., G. Masters, and F. Gilbert, Observably split multiplets: Data analysis and interpretation in terms of large-scale aspherical structure, *Geophys. J. Int., 111,* 559-576, 1992b.

Woodhouse, J. H., The coupling and attenuation of nearly resonant multiplets in the Earth's free oscillation spectrum, *Geophys. J. R. Astron. Soc., 61,* 261-283, 1980.

Woodhouse, J. H., and F. A. Dahlen, The effect of a general aspherical perturbation on the free oscillations of the Earth, *Geophys. J. R. Astron. Soc., 53,* 335-354, 1978.

Woodhouse, J. H., and T. P. Girnius, Surface waves and free oscillations in a regionalized Earth model, *Geophys. J. R. Astron. Soc., 68,* 653-673, 1982.

Woodhouse, J. H., D. Giardini, and X.-D. Li, Evidence for inner core anisotropy from free oscillations, *Geophys. Res. Lett., 13,* 1549-1552, 1986.

Zhang, Y.-S., and Tanimoto, Global Love wave phase velocity variation and its significance to plate tectonics, *Phys. Earth Planet. Inter., 66,* 160-202, 1991.

J. S. Resovsky, and M. H. Ritzwoller Department of Physics, University of Colorado, Boulder, CO 80309-0390. (e-mail: resovsky@lemond.colorado.edu)

(Received November 8, 1996; revised July 24, 1997; accepted August 27, 1997.)